 doi:10.1111/j.1471-4159.2007.04870.x

Post-synaptic density perturbs insulin-induced Kv1.3 channel modulation via a clustering mechanism involving the SH_3 domain

D. R. Marks* and D. A. Fadool*,†

*Department of Biological Science, Program in Neuroscience, Biomedical Research Facility, The Florida State University, Tallahassee, Florida, USA

†Department of Biological Science, Programs in Neuroscience and Molecular Biophysics, The Florida State University, Tallahassee, Florida, USA

Abstract

The olfactory bulb (OB) contains the highest concentration of the insulin receptor (IR) kinase in the central nervous system; however, its functional role and modulation in this region remains poorly understood. IR kinase contains a number of proline-rich motifs, making it an excellent candidate for modulation by SH_3 domain-containing adaptor proteins. Kv1.3, a voltage-gated *Shaker* potassium channel and tyrosine phosphorylation substrate of IR kinase, contains several proline-rich sequences and a canonical post-synaptic density 95 (PSD-95)/discs large/zO-1 domain (PDZ) recognition motif common to most *Shaker* family members. We sought to determine if a functional relationship existed between Kv1.3, IR kinase, and the SH_3/PDZ adaptor protein PSD-95. Through patch-clamp electrophysiology, immunochemistry, and co-immunoprecipitation, we found that while Kv1.3 and PSD-95 alone interact via the canonical C-terminal PDZ recognition motif of the channel, this molecular site of interaction acts to cluster the channels but the PSD-95 SH_3-guanylate kinase domain functionally modulates Kv1.3 activity via two proline-rich domains in its N- and C-terminal. Therefore, these data suggest that adaptor domains responsible for ion-channel clustering and functional modulation are not necessarily coupled. Moreover, IR kinase and Kv1.3 can only be co-immunoprecipitated in the presence of PSD-95 as the adapting linker. Functionally, insulin-dependent Kv1.3 phosphorylation that causes channel current suppression is blocked via interaction with the PSD-95 SH_3-guanylate kinase domain. Because all the three proteins co-localize in multiple lamina of the OB that are known to be rich in synaptic connections, membrane excitability and synaptic transmission at critical locations in the OB have the capacity to be finely regulated.

Keywords: olfactory, post-synaptic density, protein–protein interaction, receptor tyrosine kinase, trafficking, tyrosine phosphorylation.

J. Neurochem. (2007) 10.1111/j.1471-4159.2007.04870.x

Insulin and insulin receptor (IR) kinase are found in abundance in discrete brain regions yet insulin signaling in the CNS is not fully understood (Young *et al.* 1980; Wickelgren 1998; Bruning *et al.* 2000; Dickson 2003; Gerozissis 2003). The highest brain insulin-binding affinities, insulin-receptor density, and IR kinase activity are localized to the olfactory bulb (OB) (Baskin *et al.* 1983; Hill *et al.* 1986; Matsumoto and Rhoads 1990; Gupta *et al.* 1992; Banks *et al.* 1999). The large body of research on *diabetes mellitus* has elucidated the insulin-signaling system as a flexible network of interacting proteins (reviewed by Kahn 1996; White 1997; Neubauer and Kulkarni 2006) whereby a major downstream target for IR kinase and insulin growth factor receptor is insulin receptor substrate (IRS) (White 2003; Lee and White 2004). IRS has been shown to link the IR kinase with other proteins by acting as a multisite 'docking protein' to bind signal-transducing molecules containing Src homology 2 (SH_2) and SH_3 domains (Sun *et al.* 1991; Myers and White 1993). In certain areas of the brain, such as the OB, IRS is weak or absent (Folli *et al.* 1994). We have alternatively proposed that another protein substrate, a voltage-gated ion channel (Kv1.3), could serve as the interacting downstream target for brain insulin signaling, similar to IRS (Fadool *et al.* 2000; Das *et al.* 2005). Kv1.3 is a mammalian homologue of the *Shaker* subfamily (Yellen 2002), and as typical for potassium channels in general, acts to dampen the excitability of neurons by regulating the pattern and intensity of the action potential discharge. Gene-targeted deletion of Kv1.3 channel or pharmacological block of the channel in mitral (MT) cell neurons of the OB elicits increase in action potential frequency, rise time, and after

Received May 22, 2007; revised manuscript received July 5, 2007; accepted July 12, 2007.

Address correspondence and reprint requests to Debra Ann Fadool, 214 Biomedical Research Facility, Programs in Neuroscience and Molecular Biophysics, Florida State University, Tallahassee, FL 32306, USA. E-mail: dfadool@bio.fsu.edu

Abbreviations used: IR, insulin receptor; SH_3, Src homology 3; Kv1.3, voltage-gated *Shaker* potassium channel; PDZ, PSD-95/discs large/zO-1 domain; PSD-95, post-synaptic density 95; GK, guanylate kinase; IRS, insulin receptor substrate; HEK, human embryonic kidney cells; OB, olfactory bulb; MEM, minimum essential medium; SDS–PAGE, sodium dodecyl sulfate–polyacrylamide gel electrophoresis; P20, postnatal day 20; PBS, phosphate-buffered saline; co-IP, co-immunoprecipitate; MT, mitral; OSNs, olfactory sensory neurons.

hyperpolarization (Balu *et al.* 2004; Fadool *et al.* 2004). There are three tyrosine residues in the N- and C-termini of Kv1.3 that are phosphorylated by IR kinase following acute insulin stimulation of human embryonic kidney 293 cells (HEK293) co-transfected with Kv1.3 plus IR kinase (Fadool and Levitan 1998). Insulin stimulation of cloned Kv1.3 or native Kv1.3 in MT cell neurons of the OB functionally causes a suppression of the peak current amplitude without any modulation of Kv1.3 kinetics of inactivation or deactivation (Fadool and Levitan 1998; Fadool *et al.* 2000). Single channel recording of voltage-activated currents in MT cell neurons has demonstrated that the insulin-evoked Kv1.3 current suppression is attributed to a significant decrease in the open probability of the channel without any change in unitary conductance (Fadool *et al.* 2000). MT cell neurons pre-treated with pharmacological probes to block the Kv1.3 vestibule (Colley *et al.* 2004) or MT cell neurons harvested from mice with a gene-targeted deletion of Kv1.3 (Fadool *et al.* 2004) show a complete insensitivity to modulation by IR kinase, strongly suggesting that the target of insulin neuromodulation is specific to Kv1.3. Moreover, IR kinase activity is sensory-experience dependent. Animals deprived of odorant-evoked activity via unilateral naris-occlusion from birth, exhibit a decreased expression of IR kinase in the OB ipsilateral to the occlusion, and correlative MT cell neurons become insensitive to insulin (Fadool *et al.* 2000).

Insulin signaling in the adult brain may also be involved in sculpting and maintaining synaptic circuitry in addition to modulation of electrical properties of neurons. The synaptic connections in the olfactory system have long been explored because of the system's well-known capacity for continual neurogenesis (Graziadei and Monti-Graziadei 1978). Recently we found that a synaptic adaptor protein, post-synaptic density 95 (PSD-95), was strongly expressed in OB membranes (Colley *et al*., 2007) and showed increased expression in Kv1.3-null mice (Fadool *et al.* 2004). Like adaptor proteins in general, PSD-95 forms scaffolds between signaling proteins, to bring various components of a signal transduction cascade into close regulatory proximity. In particular, PSD-95 organizes protein signaling complexes at synapses and has the ability to bind numerous targets through its PDZ, SH_3, and possibly, its guanylate kinase (GK) domain (Ponting *et al.* 1997; El-Husseini *et al.* 2000; Kennedy 2000; McGee *et al.* 2001; Yaffe 2002). Much work has focused upon interactions with the PDZ domain, in particular, that interacts with the NMDA receptor to understand how the adaptor protein might regulate synaptic plasticity and learning (Kornau *et al.* 1995; Sheng 1997; Miguad *et al.* 1998; Sheng and Pak 2000; Iwamoto *et al.* 2004). PSD-95 interactions with kinases and their substrates have also been discovered (Bockmann *et al.* 2002; Kalia and Salter 2003) as well as interactions with channel auxiliary subunits via non-PDZ domain interactions (Takahashi *et al.* 2005).

The structural basis for which PSD-95 induces the clustering of voltage-gated potassium channels in the plasma membrane is widely explored (Kim *et al.* 1995; Kim and Sheng 1996; Arnold and Clapham 1999; Burke *et al.* 1999; Shin *et al.* 2000; Tiffany *et al.* 2000; Imamura *et al.* 2002). Clustering and protein–protein interactions of PSD-95 with *Shaker* channels are thought to regulate proper distribution of the channels and hence control the local excitability of the neuronal membrane (Sheng and Wyszynski 1997). At the OB synapse, the molecular mechanisms that mediate sorting, clustering, and anchoring of proteins are still largely unknown. Moreover, the functional ramifications of PSD-95 and Kv1.3 co-expression in conjunction with characterized modulatory IR kinase are unexplored. This study first explores the functional interaction of PSD-95 adaptor with the Kv1.3 ion channel and then secondly demonstrates how IR kinase modulation of the channel is perturbed in the presence of the adaptor. We report that PSD-95-mediated clustering of Kv1.3 alone is maintained via the classical PDZ-recognition motif in the C-terminal of the channel. Modulation of Kv1.3 biophysical properties by PSD-95, however, appears to be mediated through multiple molecular targets on both the channel and the adaptor, whereby mutagenesis at any one location prevents channel modulation. PSD-95-mediated clustering of Kv1.3 channel and observed co-immunoprecipitation do not appear to be coupled to the direct functional modulation of the channel. Secondly, the modulation of Kv1.3 biophysical properties induced by IR kinase are blocked by the adaptor protein PSD-95 via a mechanism attributed to the GK-SH_3 domain, which contrarily does involve adaptor-mediated clustering of the channels and the formation of a PSD-95/IR kinase/Kv1.3-channel complex. These findings demonstrate that brain IR signaling may regulate the modulation of an ion channel differently when in the presence of a synaptic adaptor protein, thus providing the use of different molecular interactions to create functional changes needed for plasticity during such neuronal activities as development, metabolism, or learning.

Materials and methods

Solutions and antisera

Human embryonic kidney 293 cell (HEK293) patch pipette solution contained (in mmol/L): 30 KCl, 120 NaCl, 10 HEPES, and 2 $CaCl_2$ (pH 7.4). HEK293 recording bath solution contained (in mmol/L): 150 KCl, 10 HEPES, 1 EGTA, and 0.5 $MgCl_2$ (pH 7.4). Cell lysis buffer with protease and phosphatase inhibitors solution contained: 25 Tris (hydroxymethyl) aminomethane (pH 7.5), 250 mmol/L NaCl, 5 mmol/L EDTA, 1% Triton X-100, 1 mmol/L sodium orthovanadate, 1 mmol/L phenylmethylsulfonyl fluoride, 10 μg/mL aprotinin, 1 μg/mL leupeptin, and 1 μg/mL pepstatin A. Wash buffer contained (in mmol/L): 25 Tris (pH 7.5), 250 NaCl, 5 EDTA, and 0.1% Triton X-100. Human recombinant insulin was purchased

from Roche (Indianapolis, IN, USA) and was used for electrophysiology at a concentration of 1 μg/mL, and for stimulation for biochemical analyses at a concentration of 10 μg/mL. αAU13, a rabbit polyclonal antiserum, was generated against a 46 amino acid sequence 478-MVIEEGGMNHSAFPQTPFKTGNSTATCTTNN-NPNDCVNIKKIFTDV-523 representing the unique coding region of Kv1.3 between the amino terminus and transmembrane domain 1 as initially characterized in heterologous expression systems (Cook and Fadool 2002), rat OB tissue (Tucker and Fadool 2002), mouse OB tissue (Colley *et al.* 2004), and in Kv1.3-null mice (Fadool *et al.* 2004). This antibody was used for immunoprecipitation (3–5 μg/1 mL lysate) and western blot detection (1 : 1000) of Kv1.3. For immunochemistry, tissue cryosections and HEK293 cells were incubated with species–specific antisera AU13/Kv1.3 (1 : 1000), PSD-95 (1 : 800), or IR_β (1 : 800) (Millipore/Upstate, Billerica, MA, USA). αIR_β is a polyclonal antibody directed against the β subunit of the human IR, which we previously characterized for cross-reactivity for cloned rIR expressed in heterologous expression systems (Fadool and Levitan 1998) and native rodent OB tissue (Fadool *et al.* 2000).

Construction of channel, IR kinase, and PSD-95 mutants

Voltage-gated *Shaker* potassium channels were expressed transiently in HEK293 cells using the Invitrogen vector $pcDNA_3$ (Carlsbad, CA, USA). Kv1.3 was ligated into $pcDNA_3$ at the unique *Hin*dIII site in the multiple cloning region, placing the channel-coding region downstream from a cytomegalovirus promoter. The IR cDNA was generously provided by Richard Roth (Stanford University, Stanford, CA, USA) in the pECE vector. The construct was subcloned into $pcDNA_3$ and a kinase-deficient IRdead was constructed by truncating 417 bases of the 3′ IR-coding region as described in Fadool *et al.* (2000) and diagramed in Fig. 1a. This mutant has an unstable β subunit, has no kinase activity *in vitro* or *in vivo* and does not mediate insulin-stimulated uptake of 2-deoxy-glucose (Ellis *et al.* 1986). Three Kv1.3 mutants were constructed to disrupt the N- and C-termini SH_3 recognition sites, and the canonical C-terminal PDZ recognition motif. For Kv1.3ΔSH_3N, prolines 41 and 42 were mutated to glycine, Kv1.3ΔSH_3C contained prolines 493 and 496 mutated to glycine, and Kv1.3ΔPDZ C-terminal ending sequence was changed from FTDV to WSAG (Fig. 1a). All Kv1.3 channel mutants were constructed with the use of two sequential PCRs. The first PCR used a mutagenic primer and an upstream primer. The second PCR used the amplified, gel-purified product of the first reaction and the downstream oligonucleotide as primers. In this way a stretch of mutant DNA flanked by two unique restriction sites was obtained; the product was double digested and ligated into the parent channel backbone with the use of T4 DNA ligase. PSD-95, contained in the vector $pcDNA_3$ (Invitrogen), was digested with *Bam*HI and *Eco*RI to remove the last 550 base pairs comprising the membrane-associated GK domain to produce PSD-95ΔGK (Fig. 1b). For PSD-95ΔSH_3, PSD-95 in $pcDNA_3$ was digested with *Bsp*120I to remove the last 1000 base pairs comprising the membrane-associated GK and the SH_3. The reactions were separated by 1% agarose gel electrophoresis, and the resulting 8100/7700 base pair bands were purified using the GeneClean II kit (Qbiogene, Morgan Irvine, CA, USA). The purified linear DNA was subcloned using a blunt-end ligation (Fig. 1b). PSD-95ΔPM was a generous gift of Dr Jeff Martens (University of Michigan) and lacks two cysteines at the N-terminus that are critical for palmitoylation and membrane targeting. PSD-95ΔPM was also tagged with the green fluorescent protein at the C-terminus (Jeff Martens, unpublished data). All mutant constructs were sequenced by the use of a cycle-sequencing reaction and an automated sequencer (Applied Biosystems Inc., Princeton, NJ, USA) to verifty the mutation and detect PCR errors.

Maintenance and transient transfection of human embryonic kidney cells

Human embryonic kidney 293 cells were maintained in minimum essential medium (MEM), 2% penicillin/streptomycin, and 10% fetal bovine serum (Gibco/Invitrogen). Before transfection, cells were grown to 95% confluency, dissociated with trypsin-EDTA (Sigma, St Louis, MO, USA) and mechanical trituration, diluted in MEM to a concentration of 600 cells/mL, and plated on Corning dishes (Catalog # 25000; Fisher Scientific, Atlanta, CA, USA). Five to 7 days after passage, cDNA was introduced into cells with a lipofectamine agent (Gibco/Invitrogen) using techniques previously described (Fadool *et al.* 1997, 2000; Cook and Fadool 2002; Colley *et al.* 2004). The lipofectamine and appropriate cDNAs were allowed to complex for 20 min, after which the HEK293 cells were transfected with the lipofectamine/cDNA complex for a period of 4–5 h in serum-reduced OptiMEM (Gibco/Invitrogen). Approximately 1 μg of each cDNA construct was used for electrophysiology, and 3 μg of each construct was used for biochemistry. In experiments where more than one cDNA was transfected, the total concentration of delivered DNA was held constant by equilibrating with empty vector ($pcDNA_3$). Cells at 40–60% confluency have been determined optimal for electrophysiology, and cells at 90% confluency work well for protein biochemistry experiments. For electrophysiology, patch-clamp experiments were performed 24–36 h post-transfection, and for biochemical experiments, cells were harvested 48 h post-transfection.

Electrophysiological techniques

Patch pipettes were fabricated from borosilicate glass (Jencons, Bridgeville, PA, USA), and were fire polished to approximately 1 μm (bubble number 5.0) (Mittman *et al.* 1987). Pipette resistances between 7 and 10 MΩ were used to produce high-resistance seals (between 8 and 14 GΩ) by applying a small amount of suction to the pipette lumen in contact with the target cell. HEK293 cells were voltage clamped at a holding potential (V_h) of −90 mV and patches were depolarized to a command voltage (V_c) of +40 mV. Macroscopic currents were recorded in the cell-attached configuration using an integrating patch-clamp amplifier (AxoPatch200B; Axon Instruments/Molecular Devices, Sunnyvale, CA, USA). The analog output was filtered between 2 and 5 kHz and digitally sampled every 0.5–4 ms. Data acquisition and analysis were carried out using pClamp 9 software (Axon Instruments/Molecular Devices). The inactivation of the macroscopic current (τ_{inact}) was fitted to the sum of two exponentials [$y = y_0 + A_1\exp(x/t_1) + A_2\exp(x/t_2)$] by minimizing the sums of squares, where y_0 is the Y offset , t_1 and t_2 are the inactivation time constants, x is the time, and A_1 and A_2 are the amplitudes. The two inactivation time constants were mathematically combined by multiplying each by its weight (A) and summing. The deactivation of the macroscopic current (τ_{deact}) was fitted similarly, but to only a single exponential ($y = y_0 + A_1\exp(x/t_1)$). The voltage-dependent activation of Kv1.3 was determined by fitting

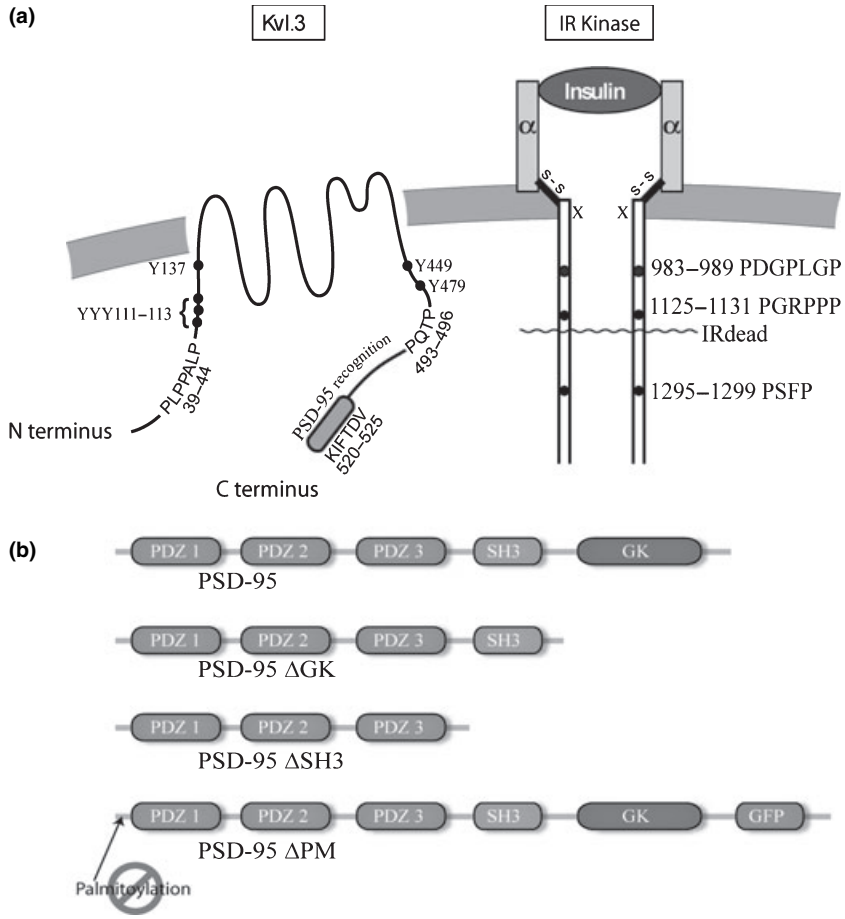

Fig. 1 Schematic representation of Kv1.3 ion channel (Kv1.3), insulin receptor (IR) kinase, and the synaptic adaptor protein post-synaptic density 95 (PSD-95). (a) Kv1.3 is a mammalian homolog of the *Shaker* subfamily of potassium channels with six transmembrane spanning regions and one pore. Note two proline-rich (P) stretches in the amino (N-terminus) and carboxyl (C-terminus) termini of the channel. (●) = tyrosine (Y) residue flanked by upstream acidic or downstream hydrophobic amino acids serving as recognition motifs for tyrosine specific phosphorylation. C-terminus gray shading = consensus sequence that binds PDZ domains contained in PSD-95. IR kinase contains two alpha subunits (α) that dimerize following ligand binding (insulin). This conformational change is translated to the β subunit linked to the α subunit via disulfide bridges (S–S) to induce autophosphorylation of multiple Y residues (not shown) on the β chain. ∼∼∼ = truncation of 417 final residues of the β chain (IRdead). Note three P stretches along the β chain. (b) Domain structure of PSD-95 and PSD-95 mutations created for this study. PDZ, PSD-95/discs large/zO-1 domain; SH_3, Src homology 3 domain; GK, guanylate kinase-like domain; GFP, green fluorescent protein; PM, palmitoylation; Δ, deleted.

current-conductance relationships with a Boltzmann expression. The Boltzmann equation that was used for fitting was: $y = [(A_1\text{-}A_2)/(1+\exp(X-X_o)/dx]+A_2]$ (Fadool *et al.* 2000; Tucker and Fadool 2002). All biophysical properties were compared using a within cell statistical design at time 0 and 30 min post-1 μg/mL insulin stimulation using a paired *t*-test at the 95% confidence level.

Protein chemistry

Immunoprecipitated proteins were separated by sodium dodecyl sulfate–polyacrylamide gel electrophoresis (SDS–PAGE) and probed by western blot analysis, as previously described (Brann *et al.* 2002; Cook and Fadool 2002). Forty-eight hours after transient transfection, HEK293 cells were stimulated with 1 μg/mL bath-applied recombinant insulin or unsupplemented media control for 8 min at 37°C. Harvested cell lysates containing expressed proteins in HEK293 cells were obtained by solubilization in ice-cold lysis buffer for 30 min at 4°C (see Solutions and antisera). The lysates were clarified by centrifugation at 14 000 *g* for 10 min at 4°C, and pre-cleared for 1 h with 3 mg/mL protein A-sepharose (Amersham-Pharmacia, Piscataway, NJ, USA). The protein of interest was immunoprecipitated from the cleared lysates by incubation overnight with 5 μg/mL of specific antibody at 4°C. The immunoprecipitates were then washed four times with wash buffer, and proteins were separated on 10% acrylamide gels by SDS–PAGE, followed by electro-transfer to nitrocellulose membranes. The nitrocellulose membranes were blocked with 5% non-fat milk and incubated overnight at 4°C with primary antibody. Membranes were then incubated with species–specific horseradish peroxidase-conjugated secondary serum for 90 min at 22°C. Labeled proteins were visualized by enhanced chemiluminesence

(Amersham/Pharmacia) and band pixel density was quantified using scanning densitometry as previously described (Tucker and Fadool 2002; Fadool *et al.* 2004). Changes in phosphorylation were quantified as a ratio (plus and minus insulin treatment) within the same autorad to control for differences in enhanced chemiluminesence exposure between experiments.

Immunochemistry

Postnatal day 20 (P20) C57B6 mice were killed via 0.2 cc pentobarbitol overdose, as approved by Florida State University Animal Care and Use Committee. Mice were perfused via cannulation with phosphate-buffered saline (PBS) (pH 7.4), followed by ice-cold 4% paraformaldehyde fixation (Acros; Morris Plains, NJ, USA). OBs were held at 4°C while they were extracted and post-fixed (4 h), followed by treatment of graded cryoprotection in 10% (2 h), 20% (2 h), and 30% (overnight) sucrose prepared in PBS. OBs were frozen in TissueTek (Electron Microscopy Sciences, Hatfield, PA, USA), 8–10 μm tissue sections were cut coronally on a Leica CM1850 microtome-cryostat (Leica; Meyer Instruments, Houston, TX, USA), and sections were stored at −20°C until use. For HEK293 immunocytochemistry, cells were fixed with St Marie's alcohol fixative for 5 min, and then washed twice in PBS. For cells and sections, non-specific binding was blocked by incubation for 30 min in PBS plus 1% Tween-20 containing 4% bovine serum albumin (PBST-Block; Sigma Chemical Co.), followed by incubation overnight at 4°C with primary antisera. Proteins were visualized using fluorescein-, rhodamine-, Texas Red-, or Cy5-conjugated secondary antisera at 40X using an Axiovert S-100 (Zeiss, Thornwood, NY, USA) equipped with epifluorescence. Images were captured using an Axiocam digital camera and Axiovision associated software. For confocal microscopy, 63–100× magnification was used on a Zeiss LSM-510 dual photon microscope with Argon, HeNe, and titanium sapphire excitation lasers (Zeiss). Transgenic mice engineered with a Thy1 promoter to drive yellow fluorescent protein expression in MT cell neurons were used to co-localize Kv1.3, IR kinase, and PSD-95 to MT cells and MT cell dendrites/axons. These were a generous gift of Dr Guopeng Feng at Duke University, as developed in the laboratory of Dr Josh Sanes (Feng *et al.* 2000).

Plot profiles of labeled HEK293 cells

Human embryonic kidney 293 cells were transfected with constructs, labeled as described above, and imaged with a 63X objective on a LSM-510 dual-photon confocal microscope with Argon, HeNe, and titanium sapphire excitation lasers (Zeiss). Pinhole diameter was opened to 1 air unit for the longest wavelength dye used, and other channel pinholes were adjusted to exactly match. Detector gain was kept strictly to 700–900 on LsMB software (Zeiss) to ensure equal exposure and capture of emission spectra. A scan average of two was used. Embedded software pixel rulers were used to find the longest cross-sectional diameter of the cell under observation to ensure each image was taken from the center of the *Z*-axis. Images were captured at 1024 × 1024 pixels resolution in LSM file format, and then were converted to a 16 bit TIFF file format using LsMB software (Zeiss). The TIFF file was opened in NIH ImageJ (Rasband 2005) and a uniform rectangle of 400 pixels × 20 pixels was applied across the midline of the cell to obtain the plot density profile of the pixels underneath. After studying plot density profiles compared with immunocytochemical data that supported strong Kv1.3 channel clustering, we set the criteria that lack of clustering was defined by the visualization of two peaks above an optical density unit of 1.0, which was the 50% interval of the density measurement. Cells that had only one peak above 1.5 optical density unit were considered to display clustering. A similar type of classification had been derived by other investigators quantifying protein localization defined by imaging data (Rubin and Katz 1999; Abramoff *et al.* 2004; Amadesi *et al.* 2006).

Results

Effects of post-synaptic density 95 on Kv1.3 ion channel function

Membrane proteins harvested from the mouse OB strongly express the adaptor protein PSD-95 and expression increases in mice with a gene-targeted deletion of Kv1.3 (Fadool *et al.* 2004). This suggests a putative signaling pathway or associated complex between the two proteins, which is perturbed in the absence of the channel. Thus we transiently co-expressed cDNA encoding Kv1.3 and PSD-95 in HEK293 cells to test any functional effects of PSD-95 on Kv1.3 biophysical properties. Macroscopic currents were recorded from cell-attached patches by typically holding the patch at rest (V_h = −90 mV) and stepping to a depolarizing voltage (V_c = +40 mV) for 1000 ms at an interpulse interval of 45 s. The time course of this protocol is routinely used in our laboratory to prevent characteristic cumulative or use-dependent inactivation of the Kv1.3 channel (Marom and Levitan 1994). Figure 2a shows a representative set of control currents generated with this voltage paradigm for a HEK cell in which the cDNA encoding Kv1.3 was singly transfected. The stability of the peak current amplitude and kinetics of inactivation was monitored shortly after obtaining the cell-attached configuration (time 0) compared with that recorded following 30 min of voltage stimulation (time 30). Channel biophysical properties were stable over the selected recording interval; neither the peak current amplitude nor the kinetics of current inactivation changed over time (Fig. 2d, Table 1). Using this same voltage paradigm, however, co-expression with PSD-95 significantly decreased the peak current magnitude of Kv1.3 by 42.1% (Fig. 2b and d) in a use-dependent fashion (Fig. 2c). The reduction in current magnitude was not attributed to a significant decrease in voltage dependence of the channel when the tail conductance was plotted against voltage and fit to a Boltzmann relationship to calculate the voltage at half-activation ($V_{1/2}$). The kinetics of inactivation (τ_{inact}) was significantly faster by 46% while there was no significant change in the kinetics of deactivation (Table 1). Interestingly, we found that channel modulation by PSD-95 was use dependent and only developed over the course of repeated stimulation. PSD-95-induced current suppression and decreased τ_{inact} was not observed if cells were voltage stimulated just once over a

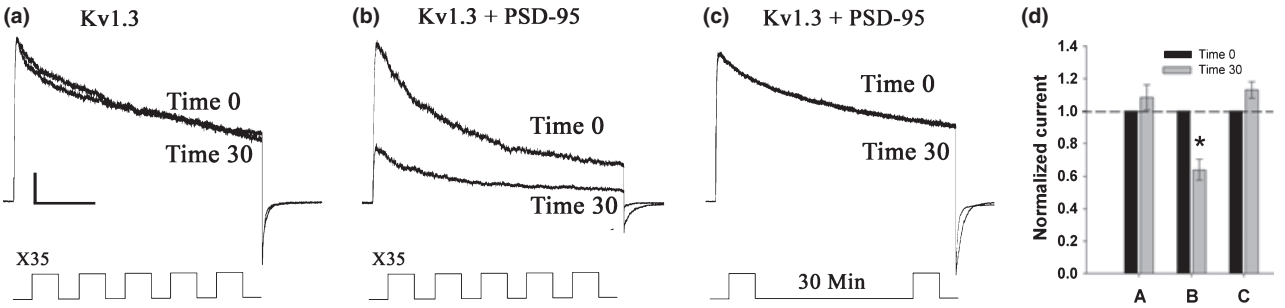

Fig. 2 Post-synaptic density 95 (PSD-95) decreases Kv1.3 inactivation (τ_{inact}) and suppresses peak current magnitude via an activity-dependent mechanism. (a–c) Representative current traces recorded from human embryonic kidney 93 cells HEK293 transiently transfected with cDNA encoding Kv1.3 channel (plus or minus adaptor). Macroscopic currents were recorded from cell-attached patches held (V_h) at −90 mV and stepped (V_c) to +40 mV for 1000 ms (P_d) using a 45 s interpulse interval (T_s). (a and b) Recorded current properties of a single cell are statistically compared after acquisition of the patch (time 0) to that recorded 30 min later (time 30) during continuous voltage stimulation (35X). (c) Same voltage paradigm in the absence of continuous voltage stimulation; T_s = 30 min. (d) Histogram summary of normalized peak current versus transfection condition in panels a, b, and c; values represent mean ± SEM, n = 8, *Statistically significant by paired t-test, $\alpha \leq 0.05$. Scale bar = 150 pA (abscissa) and 250 ms (ordinate).

Table 1 Biophysical properties of Kv1.3 channel in the presence of the synaptic adaptor, PSD-95

Condition	Time	I (pA)	τ_{inact} (ms)	$V_{½}$ (mV)	τ_{deact} (ms)	N
Kv	0	853.2 ± 151.9	629.1 ± 31.4	−40.6 ± 3.8	37.0 ± 6.3	8
	30	904.5 ± 134.3	643.7 ± 32.1	−45.7 ± 1.6	37.4 ± 6.0	
Kv + PSD-95	0	519.0 ± 133.1	705.9 ± 66.6	−44.8 ± 3.9	40.8 ± 9.7	7
	30	325.2 ± 107.0*	383.6 ± 47.0*	−49.9 ± 4.1	60.3 ± 13.9	
Kv + PSD-95 activity (−)	0	575.2 ± 156.2	749.6 ± 29.5	−44.8 ± 2.2	49.8 ± 9.6	8
	30	625.7 ± 166.8	691.0 ± 61.3	−45.9 ± 5.1	43.5 ± 9.1	
Kv + PSD-95ΔGK	0	736.6 ± 302.4	751.2 ± 70.2	−48.1 ± 3.1	46.0 ± 13.0	6
	30	727.5 ± 331.6	898.0 ± 120.3	−41.1 ± 3.7	37.4 ± 9.1	
Kv + PSD-95ΔSH_3	0	593.0 ± 155.9	550.4 ± 61.9	−44.6 ± 3.9	44.3 ± 5.5	7
	30	481.5 ± 104.2	456.4 ± 85.6	−45.1 ± 3.0	40.3 ± 5.6	
Kv + PSD-95ΔPM	0	718.7 ± 258.9	613.9 ± 76.4	−42.8 ± 2.1	38.5 ± 6.2	7
	30	742.5 ± 274.0	651.8 ± 138.9	−49.7 ± 3.0	39.8 ± 5.7	
KvΔSH_3N	0	1648.3 ± 217.2	660.5 ± 81.2	−37.7 ± 4.5	47.0 ± 8.8	6
	30	1118.1 ± 108.3*	620.4 ± 182.2	−39.6 ± 4.9	65.3 ± 16.8	
KvΔSH_3C	0	1832.1 ± 474.3	888.2 ± 135.9	−35.9 ± 3.0	34.5 ± 3.3	6
	30	1644.0 ± 353.8	657.5 ± 58.1	−38.6 ± 2.4	37.7 ± 5.7	
KvΔPDZ	0	686.16 ± 343.5	695.8 ± 62.7	−35.7 ± 1.2	30.8 ± 5.3	6
	30	639.1 ± 301.1	772.2 ± 106.6	−35.6 ± 1.7	27.8 ± 1.9	
KvΔSH_3N + PSD-95	0	1203.8 ± 229.8	566.7 ± 34.3	−42.8 ± 4.9	31.1 ± 7.4	6
	30	835.0 ± 158.9*	698.1 ± 122.9	−48.9 ± 6.2	32.1 ± 4.4	
KvΔSH_3C + PSD-95	0	1564.4 ± 400.0	877.0 ± 116.6	−49.1 ± 2.0	30.5 ± 2.6	5
	30	1393.2 ± 440.9	581.7 ± 91.2	−42.4 ± 3.5	30.2 ± 6.5	
KvΔPDZ + PSD-95	0	873.5 ± 212.3	573.2 ± 38.7	−39.9 ± 5.0	25.0 ± 3.1	6
	30	668.3 ± 154.3	567.7 ± 98.6	−44.4 ± 5.9	28.9 ± 4.1	

PSD-95, post-synaptic density 95. Values represent the mean ± standard error of the mean. *Significantly different across time (minutes) by paired t-test ($\alpha \leq 0.05$) within transfection condition (Condition). Patches were held (V_h) at −90 mV and stepped (V_c) to +40 mV for a pulse duration (P_d) of 1000 ms using an interpulse interval of 45 s. For the calculation of inactivation (τ_{inact}), deactivation, (τ_{deact}), and voltage at one-half activation ($V_{1/2}$), please see text.

half-hour recording interval (Fig. 2c, Table 1), suggesting a property of use-dependent modulation.

Voltage-gated *Shaker* potassium channel is a substrate for phosphorylation by both receptor and cellular tyrosine kinases as well as serine/threonine kinases to induce changes in peak current magnitude, kinetics of inactivation, or surface expression (Kupper *et al.* 1995; Holmes *et al.* 1996a; Bowlby *et al.* 1997; Fadool *et al.* 1997; Fadool and Levitan

1998; Fadool *et al.* 2000; Cook and Fadool 2002; Tucker and Fadool 2002; Colley *et al.* 2004; Colley *et al*., 2007). Kv1.3 and Kv1.5 channels also have conserved proline rich sequences (PXXP) in the proximal N- and C-termini that serve as recognition motifs for SH_3-domain binding (Fig. 1a) (Holmes *et al.* 1996a, b; Cook and Fadool 2002; Nitabach *et al.* 2002) via a phosphorylation-independent mechanism. The GK domain of membrane-associated guanylate kinases (MAGUK family proteins) lacks several critical residues involved in ATP binding and catalysis and no kinase function has been definitively demonstrated (Yaffe 2002). We hypothesized, therefore, in co-transfection conditions with only Kv1.3 plus PSD-95, that closely associated protein interactions with the channel might be responsible for the observed changes in channel current rather than phosphorylation. To test this hypothesis, we disrupted the potential SH_3 recognition sites in the proximal N- and C-termini of the channel (referred to as Kv1.3ΔSH$_3$N and Kv1.3ΔSH$_3$C, respectively) using P to G substitution in the PXXP motifs (Fig. 1a). Likewise, we also constructed a channel mutation in the terminal PDZ recognition motif (Kv1.3ΔPDZ) that also would disrupt a different phosphorylation-independent interaction. Representative control recordings taken from HEK cells singly transfected with these three-channel mutations and stimulated with the same voltage protocol as previously described are shown in Fig. 3, panels a–c. Disruption of the proximal N-terminal, tandem PXXPXXP site changed the stability of the basal current amplitude that ran down over

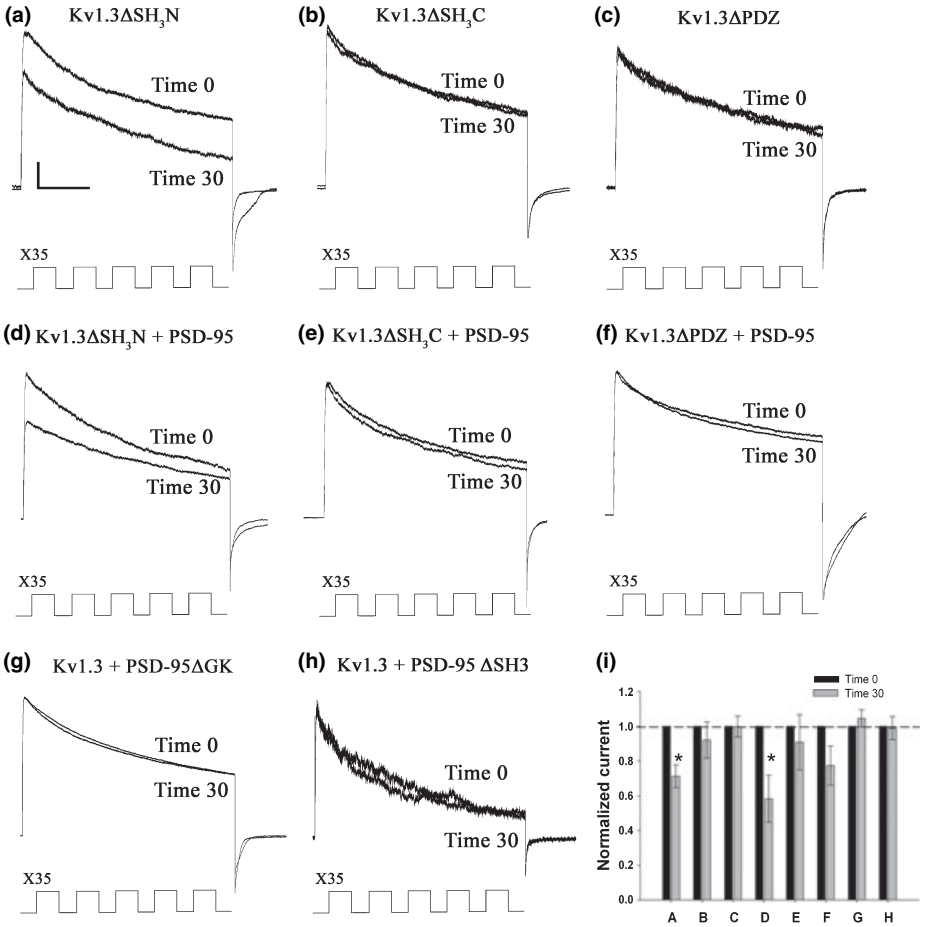

Fig. 3 Post-synaptic density 95 (PSD-95) modulation of Kv1.3 current relies upon the Src homology 3 domain (SH_3)–guanylate kinase-like domain (GK) of PSD-95 and the proline-rich domains in the C- and N-termini of Kv1.3. (a–h) Representative current traces recorded from human embryonic kidney 293 cells (HEK293) transiently transfected with cDNA encoding Kv1.3 channel (plus or minus adaptor). Macroscopic currents were recorded from cell-attached patches held (V_h) at −90 mV and stepped (V_c) to +40 mV for 1000 ms (P_d) using a 45 s interpulse interval (T_s). See text for notation of adaptor and channel mutations. Shown are various transfection conditions whereby the recorded current properties of a single cell are statistically compared after acquisition of the patch (time 0) to that recorded 30 min later (time 30) during continuous voltage stimulation (35X). (d) Histogram summary of normalized peak current versus transfection condition in panels a–h; values represent mean ± SEM, n = 5–8, *Statistically significant by paired t-test, $\alpha \leq 0.05$. Scale bar = 250 pA (abscissa) and 250 ms (ordinate).

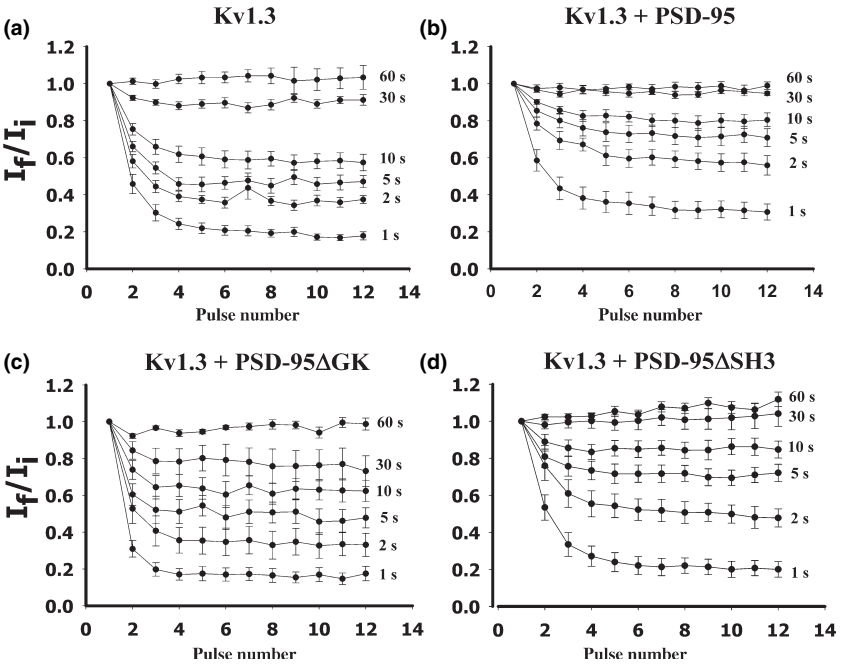

Fig. 4 Cumulative inactivation of Kv1.3 is modulated by the GK domain of post-synaptic density 95 (PSD-95). Human embryonic kidney cells (HEK) 293 cells were variously transfected as noted. Cells were voltage clamped in the cell-attached configuration with V_h = −90 mV and V_c = +40 mV for 1000 ms (P_d) with different interpulse intervals (T_s) including 60, 30, 10, 5, 2, and 1 s. Peak current amplitudes were normalized to that of the first voltage stimulation (I_f/I_i), and this normalized current was plotted against pulse number. Error bar represents mean ± SEM for 6–8 cells recorded at a given T_s.

time in the Kv1.3ΔSH$_3$N transfection condition (Fig. 4a, Table 1). We also noted that mutation of either proline rich site (Kv1.3ΔSH$_3$N or Kv1.3ΔSH$_3$C) significantly enhanced (twofold) the basal current amplitude of the channel (Table 1). If these proline-rich sites serve also as PY motifs for ubiquitin protein ligases (Henke *et al.* 2004) as well as SH$_3$-binding sites, disruption of the motif might secondarily increase the half-life of the channel in the membrane via blocked ubiquitination, consistent with an increase in basal current amplitude. Co-transfection of PSD-95 with any of the three-channel mutants failed to either decrease peak current magnitude or τ_{inact} as was previously observed for the wildtype channel (Fig. 4d–f). Because of the changes in basal channel properties upon disruption of one of the proline-rich domains (Kv1.3ΔSH$_3$N construct), we oppositely removed similar interaction domains on the adaptor while leaving the channel unchanged. We constructed a PSD-95 truncation in which only the three PDZ domains were retained and both the GK and SH$_3$ domains were removed (PSD-95ΔSH$_3$) and one in which just the GK domain was removed (PSD-95ΔGK) (see Fig. 1b). While most recently structural studies have demonstrated a PSD-95 GK consensus binding motif in other proteins (rationale for truncation of just the GK domain; PSD-95ΔGK), the SH$_3$ and GK domains are known to be an integrated folded unit and strong evidence has demonstrated that intramolecular interactions are very important for scaffold organization, thus the rationale for mutating the SH$_3$–GK as a cluster (PSD-95ΔSH$_3$, see Fig. 1b) (McGee *et al.* 2001; Tavares *et al.* 2001; Reese *et al.* 2007). Co-transfection of either of these mutant PSD-95 cDNA constructs with wildtype Kv1.3, again resulted in abolishing the modulation (Fig. 3g–i). Collectively, the experiments contained in Fig. 3 suggest that multiple sites of interaction can mediate PSD-95-induced changes in Kv1.3 activity. Channel mutation of the suspected amino terminal PDZ-recognition site or the proline-rich SH$_3$ binding sites both appear to functionally disrupt the channel modulation.

If channel modulation by PSD-95 was use dependent, we questioned whether PSD-95 was also altering use dependent or cumulative inactivation kinetics of Kv1.3 (Marom and Levitan 1994). Kv1.3 ion channel exits the inactivated state relatively slowly compared with other *Shaker* subfamily members (Panyi *et al.* 1995; Levy and Deutsch 1996), whereby interpulse intervals < 60 s can produce cumulative inactivation upon repeated stimulation. HEK293 cells transfected with only Kv1.3 were therefore subjected to a series of 12 stepwise depolarizations from −90 mV to +40 mV with varying short interpulse intervals. Interpulse intervals of 60, 30, 10, 5, 2, and 1 s were used in succession on each HEK293 cell obtained. These exact protocols were then repeated on a set of HEK293 cells co-transfected with Kv1.3 + PSD-95, Kv1.3 + PSD-95ΔGK, or Kv1.3 + PSD-95ΔSH$_3$. Peak current amplitudes at each pulse number (I_f) were normalized to that of the initial current magnitude of the first pulse (I_i) for individual patches. Mean ratios were plotted for each of the tested interpulse intervals acquired for each of the four transfection conditions (Fig. 4). Kv1.3 transfected cells begin to show slight cumulative inactivation using a 30 s interpulse interval with a strongly developed

cumulative inactivation between 10 and 1 s interpulse intervals (Fig. 4a). With a 2 s interpulse interval as many as 60% of the channels are found in the inactivated state and fail to be opened upon voltage stimulation. PSD-95 co-transfection moderately disrupts this pattern of Kv1.3 cumulative inactivation as plotted in Fig. 3b. There is no cumulative inactivation using 30 s interpulse intervals and only about 40% of the channels are in the inactivated state with a 2 s interpulse interval. Substitution using the PSD-95ΔGK mutant in the transfection scheme, did not significantly modify cumulative inactivation compared with the Kv1.3 only condition (Fig. 4c). Further truncation into the SH_3–GK domain (PSD-95ΔSH_3 construct; Fig. 4d) produced a plot that closely resembled that of Kv1.3 + PSD-95 (Fig. 4b). These data suggest that the GK domain but not the SH_3–GK domain is required in modulating the cumulative inactivation property of Kv1.3 channels. Although countertuitive, removal of just the GK domain (PSD-95ΔGK) versus removal of the combined SH_3–GK domain (PSD-95ΔSH_3) cannot be considered as linear domains or 'beads on a string' as coined by Reese *et al.* (2007), because of changed (differential) SH_3–GK intermolecular regulation of the three PDZ domains present in both of the mutant PSD-95 constructs when either the GK or combined SH_3–GK domains are disrupted.

Post-synaptic density 95 disrupts insulin receptor kinase modulation of Kv1.3 activity

We had previously demonstrated that IR kinase phosphorylates Kv1.3 at multiple *Y* residues ($Y^{111–113}$, Y^{137}, and Y^{449}) to invoke suppression of peak current amplitude without changing the voltage dependence, kinetics of inactivation, or kinetics of deactivation of the channel (Fadool *et al.* 2000). Such a modulation is thought to be attributed to the transfer of the negatively charged phosphate moiety and does not require an IR kinase/Kv1.3 association (Fadool and Levitan 1998; Fadool *et al.* 2000). The β chains of IR kinase contain several proline-rich domains (amino acids 983–989, 1125–1131, 1295–1299, see Fig. 1a) that might interact with the SH_3 domain of PSD-95 to alter IR kinase-induced modulation of Kv1.3. Adaptor proteins nShc and Grb10 contain a similar array of proline-rich stretches that can bind to Src kinase to differentially perturb Src- and TrkB-induced modulation of Kv1.3 (Cook and Fadool 2002; Beverly Colley, unpublished data). Therefore to strengthen the general paradigm that adaptor proteins alter kinase-induced modulation of Kv1.3 current properties through decreased current suppression and reduced phosphorylation, we co-expressed Kv1.3 + IR in the presence or absence of PSD-95. Figure 5a shows representative current traces recorded from a HEK293 cell held at −90 mV and stepped to a depolarizing

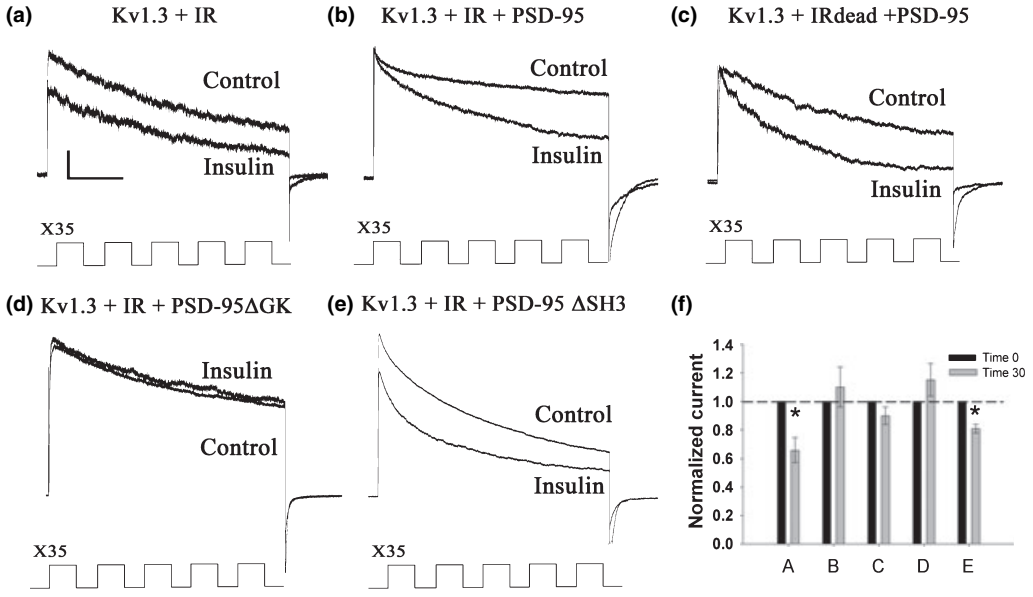

Fig. 5 Insulin-evoked Kv1.3 current suppression is blocked by post-synaptic density 95 (PSD-95) via its Src homology 3 domain (SH_3)–guanylate kinase-like domain (GK). Human embryonic kidney 293 cells (HEK293) were variously transfected as noted. (a–e) Cells were voltage clamped in the cell-attached configuration with V_h = −90 mV and V_c = +40 mV for 1000 ms (P_d) with an interpulse interval (T_s) of 45 s. Each recording represents a single patch with repeated current measure prior and following 30 min ligand (insulin) stimulation. Patch pipettes were tip-filled with control patch solution (*control*) and back-filled with 1 μg/mL of insulin (*insulin*) to phosphorylate the Kv1.3 channel over time (x35 voltage stimulations). (f) Histogram summary of normalized peak current versus transfection condition in panels a–e; values represent mean ± SEM, n = 6–9, *Statistically significant by paired *t*-test, $\alpha \leq 0.05$. Scale bar = 100 pA (abscissa) and 250 ms (ordinate).

potential of +40 mV using the above described interpulse interval of 45 s and pulse duration of 1000 ms, for 35 stimulations. The patch pipette was tip-filled with control patch solution and then backfilled with 1 μg/mL of insulin to allow phosphorylation of the Kv1.3 channel with time (Fadool *et al.* 2000). *Control* represents the first current trace recorded at time 0 and *Insulin* represents the final current trace recorded after a repetitive series of voltage sweeps. Initial current magnitude (control) was compared with that measured 30 min post-insulin stimulation (insulin), and as previously reported (Fadool *et al.* 2000; Colley *et al.* 2004), was found to be significantly decreased by 44 ± 9% (Fig. 5a and f; Table 2). Applying the same voltage paradigm and analysis, co-transfection of PSD-95 cDNA with that of Kv1.3 + IR failed to elicit the IR kinase-induced current suppression when stimulated with insulin and additionally caused a 50% decrease in the τ_{inact} (Table 2; Fig. 5b and f). If we did not backfill with insulin but substituted normal patch pipette solution, then PSD-95 evoked a similar decrease in the inactivation time constant but was now not capable of reversing the IR kinase-induced suppression of Kv1.3 current (data not shown). In contrast, if we blocked IR kinase activation by truncating the β chain and eliminating catalytic activity (IRdead), then PSD-95 co-transfection failed to evoke the IR kinase-induced Kv1.3 current suppression, but did show the decrease in inactivation kinetics (Table 2; Fig. 5c). These data suggest that reversal of Kv1.3 current suppression and not the kinetics of inactivation may be dependent upon the dimerization of the IR kinase upon binding insulin in the presence of PSD-95. IRdead is still able to bind insulin and dimerize, however, no kinase activity is possible. We have previously demonstrated that IRdead has no functional or catalytic ability to modulate or phosphorylate Kv1.3 alone in the absence of PSD-95 (Fadool *et al.* 2000).

If the PSD-95 block of IR kinase-induced Kv1.3 current suppression (Fig. 5b) was mediated by possible PSD-95 interactions with IR kinase, it should be possible to uncouple such a functional complex by eliminating either the GK (PSD-95ΔGK) or both the GK and SH_3 domains (PSD-95ΔSH_3). By substituting these two PSD-95 mutants in the co-transfection scheme, IR kinase-induced Kv1.3 current suppression was still blocked when Kv1.3 + IR was co-transfected with PSD-95 ΔGK (Fig. 5d) but suppression was regained when Kv1.3 + IR was co-transfected with PSD-95ΔSH_3 (Fig. 5e and f). These data suggest that the GK domain of PSD-95 can mediate the interaction between the adaptor/kinase/channel that decreases Kv1.3 τ_{inact} but that the combined SH_3–GK domain is necessary to additionally prevent IR kinase-evoked Kv1.3 current suppression. This mechanism must be distinct from the PSD-95-induced Kv1.3 alone modulation (Figs 2b, 3g and h) where both reduction of current magnitude and decreased τ_{inact} is lost if just the GK domain is removed (Fig. 3g).

Molecular domains, permitting the assembly of a Kv1.3/IR kinase/PSD-95 scaffold complex, block Kv1.3 phosphorylation but promote co-immunoprecipitation following IR kinase activation by insulin

Co-immunoprecipitation of *Shaker* and membrane-associated guanylate kinases family members has been well characterized (Kim *et al.* 1995). As predicted, we were able to document such a protein–protein interaction between Kv1.3 and PSD-95 in the OB, a tissue that is enriched in Kv1.3 protein (Fig. 6a). OB whole-cell lysates were prepared from P20 mice and immunoprecipitated with either control rabbit sera (lane 1) or an antiserum to Kv1.3 (lane 2). Lysates were then separated by SDS–PAGE, electro-transferred to nitrocellulose and probed with α-PSD-95. PSD-95 expression in the Kv1.3 immunoprecipitated OB lysates was primarily detected at the expected molecular mass of 97 kDa but all three isoforms of the adaptor (97, 72, and 63 kDa) could be resolved when higher concentrations of protein sample were loaded for electrophoretic separation. As a migration caliber, cloned PSD-95/Kv1.3 complex was detected in similarly treated lysates prepared from co-transfected HEK293 cells (lane 3). As an additional control for specificity, PSD-95 could be detected in OB lysates from Kv1.3−/− animals

Table 2 Biophysical properties of Kv1.3 channel plus IR kinase in the presence of the synaptic adaptor, PSD-95

Condition	Time	*I* (pA)	τ_{inact} (ms)	$V_{½}$ (mV)	τ_{deact} (ms)	*N*
Kv + IR	0	565.0 ± 171.5	688.0 ± 20.9	−49.8 ± 4.7	47.5 ± 5.0	8
	30	132.8 ± 129.0*	665.5 ± 21.6	−53.5 ± 3.6	51.5 ± 7.7	
Kv + IR + PSD-95	0	397.1 ± 120.5	715.0 ± 33.6	−44.7 ± 1.8	40.8 ± 5.2	9
	30	438.5 ± 135.7	397.5 ± 45.9*	−54.7 ± 2.7	62.6 ± 6.5	
Kv + IRdead + PSD-95	0	359.2 ± 53.4	728.6 ± 37.7	−41.9 ± 6.0	43.7 ± 6.1	8
	30	340.0 ± 53.4	390.9 ± 22.6	−55.2 ± 5.2	52.0 ± 6.3	
Kv + IR + PSD-95ΔGK	0	303.1 ± 77.9	569.7 ± 22.9	−38.1 ± 3.1	71.5 ± 16.4	6
	30	390.5 ± 84.2	586.4 ± 64.5	−41.1 ± 3.7	56.4 ± 17.1	
Kv + IR + PSD-95ΔSH_3	0	738.0 ± 295.5	686.4 ± 70.3	−49.2 ± 3.5	36.1 ± 5.3	9
	30	620.4 ± 247.7*	661.6 ± 97.8	−48.3 ± 3.0	36.2 ± 5.1	

All notations as in Table 1.

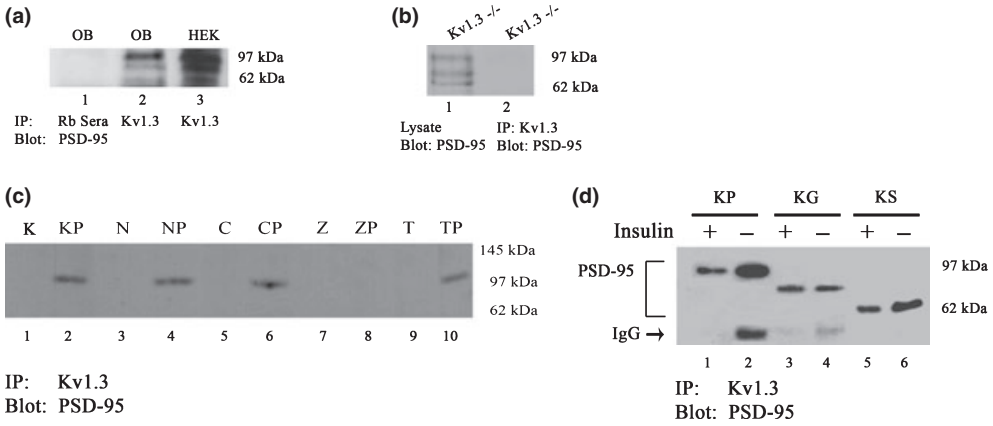

Fig. 6 Molecular domains permitting the assembly of a Kv1.3/post-synaptic density 95 (PSD-95) scaffold complex. (a) Mouse olfactory bulb (OB) lysates (lanes 1 and 2) or lysates prepared from human embryonic kidney 293 cells (HEK 293) (lane 3) co-transfected with Kv1.3 and PSD-95 were immunoprecipitated (IP) with either rabbit sera (Rb Sera) or αAU13 (Kv1.3), an antibody directed against the Kv1.3 channel. Proteins were separated by 10% sodium dodecyl sulfate–polyacrylamide gel electrophoresis (SDS–PAGE) and electro-transferred to nitrocellulose. Nitrocellulose blots were probed with antiserum for post-synaptic density 95 (blot: PSD-95) (1 : 1000). (b) OB lysates were prepared from Kv1.3–/– mice. Lane 1 = blot: PSD-95 (1 : 1000). Lane 2 = IP: Kv1.3, blot: PSD-95. (c) HEK293 cells transfected with wildtype Kv1.3 (K) channel, or one of the following four mutant channels: Kv1.3ΔSH$_3$N (N), Kv1.3ΔSH$_3$C (C), Kv1.3ΔPDZ (Z), or C455M Kv1.3 (T) minus or plus PSD-95 (P). Cells were then harvested, immunoprecipitated, separated, and probed with antisera as in (a). (d) HEK293 cells co-transfected with Kv1.3 (K) and either wildtype (P), guanylate kinase (G) deficient, or SH$_3$–GK domain deficient (S) PSD-95 constructs as indicated with (+) and without (–) 10 min insulin (10 μg/mL) stimulation. Cells were then harvested, immunoprecipitated, separated, and probed with antisera as in (a).

(Fig. 6b, lane 1), but the PSD95/Kv1.3 complex failed to be immunoprecipitated (lane 2) when samples were immunoprecipitated with αKv1.3 and blotted with αPSD-95. We next questioned whether the Kv1.3/PSD-95 protein interaction required solely the traditional C-terminal consensus sequence TDV, or whether the SH$_3$–GK domain of PSD-95 was additionally involved. Figure 6c (lanes 1 and 2) demonstrates that the channel (K) and adaptor protein (P) can be co-immunoprecipitated as expressed in HEK293 cells. Mutation of the PXXP motif in either the proximal N- or C-terminus (Kv1.3ΔSH$_3$N = (N); Kv1.3ΔSH$_3$C = (C); Fig. 6, lanes 3–6) fails to block co-immunoprecipitation, even though it prevents functional modulation. Substitution of PSD-95 constructs lacking either the GK [PSDΔGK = (G)] or the SH$_3$–GK domains [PSDΔSH$_3$ = (S)] also did not disrupt the channel/adaptor complex (Fig. 6d). Mutation of the C-terminal PDZ-binding motif of the channel [Kv1.3ΔPDZ = (Z)], however, prevented co-immunoprecipitation (Fig. 6c, lanes 7 and 8). As an additional control, a cysteine to methionine point mutation was constructed at amino acid 455 (T) of the channel to ensure any disruption near the proline SH$_3$ targets or cytoplasmic tyrosine phosphorylation sites did not have a non-selective effect in perturbing the Kv1.3/PSD-95 association (Fig. 6c, lanes 9 and 10). These data indicate that the PSD-95/channel association is via the PDZ domains and the traditional Kv1.3 C-terminal consensus sequence TDV (Fig. 1). The association of the complex, however, is not tightly coupled to PSD-95-evoked Kv1.3 functional modulation. Domains not necessary for co-immunoprecipitation can modulate Kv1.3 current properties, as can those necessary for complex formation.

Voltage-gated *Shaker* potassium channel and receptor tyrosine kinases (TrkB or IR kinase) fail to be co-immunoprecipitated in the absence of an adaptor protein serving as a molecular linker between the two proteins (Debra Fadool, unpublished data). Therefore, we wondered if Kv1.3 and IR kinase would co-immunoprecipitate (co-IP) in the presence of PSD-95 and, conversely, if demonstrated Kv1.3/PSD-95 interaction supported by Fig. 6a–d would be lost via expression of an interflanking IR kinase. As shown in Fig. 7a, HEK293 cells transfected with Kv1.3 channel + IR kinase (lanes 3 and 4) and ±PSD-95 (lanes 13–20), were immunoprecipitated with αKv1.3 and blotted first with αPSD-95, then the nitrocellulose was stripped and reprobed with αIR$_\beta$. Results (Fig. 7a, top panel) indicate that the Kv1.3/PSD-95 complex is not interrupted by IR kinase co-expression nor altered by insulin stimulation, whether the PSD-95 cDNA is full length (P) or truncated to remove the GK (G) or SH$_3$–GK domain (S). Note that palmitoylation of the PSD-95 adaptor (M) is essential for Kv1.3/PSD-95 complex association as suggested by the fact that the channel and PSD-95 palmitoylation mutant fail to co-IP whether or not IR kinase is present (Fig. 7a, lanes 11–12, 19–20). Results also confirm that Kv1.3 does not directly co-IP with IR kinase (lanes 3 and 4, bottom panel); however, the

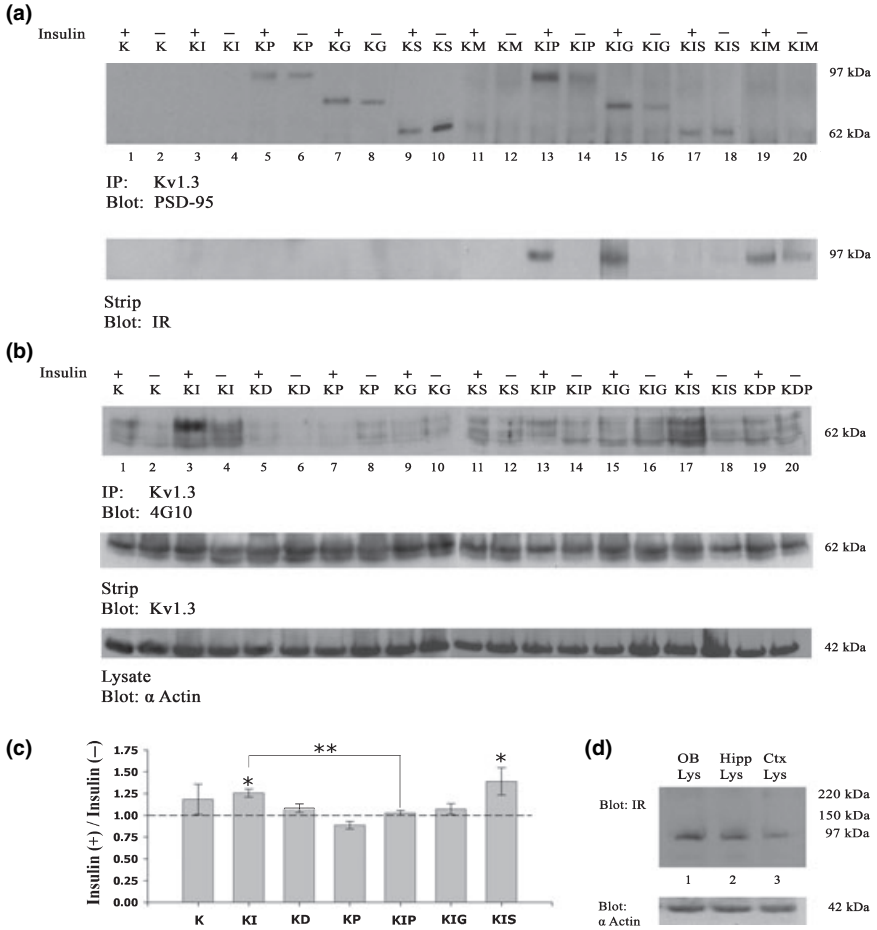

Fig. 7 Molecular domains and phosphorylation dependence permitting assembly of a Kv1.3/IR kinase/post-synaptic density 95 (PSD-95) scaffold complex. (a) HEK293 cells co-transfected with the following primary transfection conditions – Kv1.3 (K); Kv1.3 plus IR kinase co-transfected (KI); Kv1.3 plus PSD-95 co-transfected (KP); Kv1.3, IR kinase, and PSD-95 co-transfected (KIP). Transfections also incorporated the following PSD-95 mutant constructs – PSD-95 Δ GK (G), PSD-95 ΔSH_3 (S), PSD-95 Δ PM (M). Lysates were immunoprecipitated with αAU13 (IP: Kv1.3) and then probed for PSD-95 (blot: PSD-95). Nitrocellulose was then stripped and reprobed for IR kinase (M_r = 97 kDa) using an antiserum directed against the β-subunit (blot: IR_β) (1 : 1000). Note that IR kinase does not affect the co-IP of channel and adaptor but that the channel and kinase cannot be co-immunoprecipitated in the absence of the adaptor. Note also that formation of complex is augmented by 10 min insulin (10 μg/mL) stimulation over that of vehicle control (–). (b) Same as in (a) except prepared lysates were immunoprecipitated with αAU13 (IP: Kv1.3) and probed with α4G10 (blot: 4G10) (1 : 1000) that recognizes tyrosine phosphorylated proteins. Nitrocellulose was then stripped and reprobed with αAU13 (blot: Kv1.3) to demonstrate equivalent protein expression of the channel in each transfection condition. Lysate input for IP was additionally probed with αactin (1 : 800) to insure equivalent protein concentration of prepared lysates. (c) Histogram representation of the change in phosphorylation of Kv1.3 under insulin stimulation/unstimulated conditions. Densitometric ratio of 1.0 (no difference) is denoted by the dashed line. *Significantly different, Student's *t*-test (arc-sin transformation of percentage data). Plotted is the mean ratio ± SEM, $n = 4$. **One-way ANOVA with Tukey follow-up test. (d) Mouse olfactory bulb (OB), hippocampus (Hipp), and cerebral cortex (Ctx) lysates were separated as in (Fig 6a) and blotted with αR_β (1 : 1000). Nitrocellulose was then stripped and reprobed for αactin (1 : 800).

channel will co-IP with PSD-95 alone (lanes 5 and 6) and will co-IP with IR kinase in the presence of PSD-95 (Fig. 7a, bottom panel, lane 13). Note that 10 min bath stimulation with 10 μg/mL of insulin (+) prior to cell lysis compared with that of vehicle control (−) is required for IR kinase to co-IP with the channel in the presence of PSD-95 (lanes 13 and 14, bottom panel), and that the SH_3, but not GK domain (lanes 15–18, bottom panel), mediates this complex. Lastly, a series of transfection conditions were compared to determine the tyrosine phosphorylation dependence of the protein–protein interaction. Prepared lysates were immunoprecipitated with αKv1.3 and then nitrocellulose was blotted with α4G10, a monoclonal antiserum that recognizes tyrosine phosphorylated residues. As shown in Fig. 7b (lanes 3 and 4) and analyzed via quantitative densitometry in Fig. 7c, insulin stimulation of Kv1.3 + IR kinase co-transfected HEK293

cells causes an increase in channel phosphorylation that is not dependent upon co-immunoprecipitation (Fig. 7a, lanes 3 and 4). Substitution of the IRdead mutation effectively eliminates the insulin-evoked channel phosphorylation (lanes 5 and 6). Interestingly, the Kv1.3 + IR + PSD-95 transfection condition, where all proteins were demonstrated to co-IP (Fig. 7a, lanes 13 and 14), demonstrates no basal or insulin-stimulated phosphorylation of the channel (Fig. 7b, lanes 13 and 14; Fig. 7c), suggesting that complex assembly blocks IR kinase induced-Kv1.3 phosphorylation. If both the GK and SH_3 domains are removed (S), insulin-evoked Kv1.3 phosphorylation is restored, indicating that the SH_3–GK domain may be the site of complex interaction that is blocking IR kinase induced-Kv1.3 phosphorylation in the presence of PSD-95 (Fig. 7b, lanes 13–18). Finally, note that in the Kv1.3 + PSD-95 transfected condition, where expressed proteins were demonstrated to co-IP, that the channel is not phosphorylated, either basally or insulin stimulated (Fig. 7b, lanes 7 and 8), suggesting that the intact GK kinase domain is not changing the Y phosphorylation of the channel that is detectable in the wild-type channel.

Molecular domains required for PSD-95 clustering of Kv1.3 ion channels and IR kinase in the presence of Kv1.3

The conserved C-terminal sequence (-TDV) of *Shaker* subfamily members serves as a binding site for the second and third PDZ domains of the PSD-95 adaptor (Kim *et al.* 1995; Doyle *et al.* 1996; Songyang *et al.* 1997; Imamura *et al.* 2002) to promote high-density clustering of potassium channels in specific microdomains of the neuronal membrane (Ponting *et al.* 1997; Arnold and Clapham 1999). The fact that there is a great diversity in clustering efficiency across subfamily members suggests that interactions with PSD-95 that promote clustering must involve more than just these last three residues (Kim and Sheng 1996). We questioned whether PSD-95-induced clustering of Kv1.3 was mediated by the molecular domains found to induce modulation of channel function (SH_3–GK domain). Secondarily we also wanted to test whether PSD-95 clustering of Kv1.3 channels could be disrupted by IR kinase.

Differential clustering efficiency has been reported across the subfamily members (Kim and Sheng 1996) and few studies have explored the mechanistic basis of Kv1.3 clustering in particular (Kim and Sheng 1996; Hanada *et al.* 1997; Cayabyab *et al.* 2000), thus we initiated these next series of confocal imaging experiments in HEK293 cells utilizing heterologous expression of channel/adaptor or channel/adaptor/kinase cDNA constructs. As shown in Fig. 8a, the uniform distribution of Kv1.3 throughout the cell membrane was predominantly clustered in a portion of the cell membrane upon co-transfection of full length PSD-95 (Fig. 8b, part I). We suspect that the relatively large nucleus in HEK293 cells is likely promoting this unipolar pattern of clustering. Also note that Kv1.3 robustly expresses in HEK293 cells and can promote a rounded up morphology that does not affect the surface distribution of the channel (Fig. 8, part IV) compared with its native, more fusiform cell shape. While it can be observed that not all cells are uniformly rounded in morphology, we elected to image these types of transfected cells (a–m) to facilitate ease of plot intensity profile analysis (parts I–III). The distinct pattern demonstrated by the pixel plot intensity profile (see Materials and methods) can be quantitatively compared across these transfection conditions as in Fig. 8, part I. Substitution of either mutant PSD-95 cDNA in the transfection scheme did not prevent the channel clustering (Fig. 8c and d, part I) but mutation of the palmitolyation capacity of PSD-95 had a strong effect and prevented both clustering of Kv1.3 as well as proper surface expression of the adaptor (Fig. 8e, part I). As modulation of Kv1.3 by PSD-95 exhibited use dependence, we co-transfected a non-conducting Kv1.3 that was created by point substitution of a tryptophan amino acid in a critical pore position of the channel (W386F Kv1.3) (Perozo *et al.* 1993; Holmes *et al.* 1997). The plot intensity profile of W386F Kv1.3 was not significantly different from that of wild-type WT Kv1.3 (Fig. 8a and f, parts I and II), nor was the ability of the adaptor protein to cluster W386F Kv1.3 modified in the absence of potassium conductance (Fig. 8g, part II). These collective data suggest that the recorded functional PSD-95 modulation of Kv1.3 is likely not accomplished via channel clustering. This is in contrast to what was observed for PSD-95-evoked clustering of Kv1.3 in the presence of insulin. Here, the pattern of membrane expression of IR kinase (IR) is not altered via single co-expression of Kv1.3 or via PSD-95 (Fig. 8h, part III). However, if all three constructs are co-expressed, PSD-95 has the ability to cluster IR kinase (Fig. 8j) and this is not dependent upon the GK domain (Fig. 8k) but rather upon the GK-SH_3 domain (Fig. 8l, part III). These data suggest that the clustering of IR kinase that is dependent upon a Kv1.3/IR kinase/PSD-95 protein–protein interaction allows PSD-95 block of insulin-induced Kv1.3 current suppression.

Kv1.3 channel, PSD-95 adaptor protein, and IR receptor tyrosine kinase co-localize widely to several cell types across the neural lamina of the olfactory bulb

Voltage-gated *Shaker* potassium channel current suppression and decreased τ_{inact} would be predicted to increase the excitability of neurons by altering the underlying K-channel contribution to evoked action potentials. Co-localization of Kv1.3 with IR kinase and PSD-95 in the OB to specific neuronal cell types could provide a guideline as to putative function of the modulation. P20–P30 C57B6 mice were anesthetized by pentobarbitol, perfused with 4% paraformaldehyde, and the OBs were quickly removed. Tissue was post-fixed and sucrose protected for cyrosectioning as described (see Materials and methods). Sections were labeled

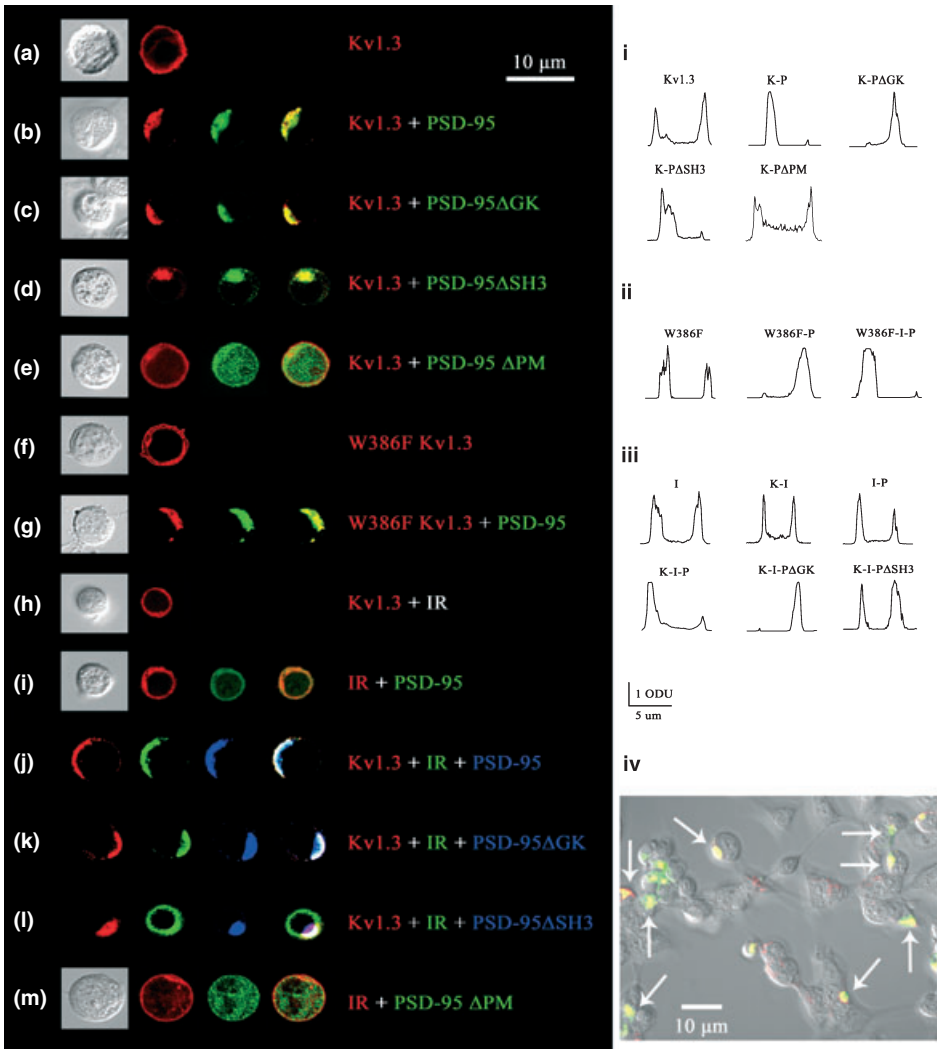

Fig. 8 Molecular domains required for post-synaptic density 95 (PSD-95) clustering of Kv1.3 ion channels and the clustering of IR Kinase in the presence of Kv1.3. (a–m) Representative confocal photomicrographs of HEK293 cells transfected with indicated cDNAs and imaged using immunochemical protocols to visualize the distribution of the protein of interest. Transfected conditions are color-coded with the reflected light observed in conjunction with the respective secondary antisera used and the applied excitation spectra. In panels where dual or triple labeling was performed, the final panel of the set represents the merged image (either yellow or white). All notations as in Fig. 1; W386 F Kv1.3 = non-conducting Kv1.3 construct. These images were representative of at least three individual transfections and image analysis of at least 4 cells per transfection condition. Scale bar = 10 μm. (I–III) Plot density profiles of immunofluorescent signals acquired from the HEK293 cells transfected with indicated cDNAs. Lack of clustering was defined by the visualization of two peaks above an optical density unit (ODU) of 1.0, which was the 50% interval of the density measurement. Cells that had only one peak above 1.5 ODU were considered to display clustering. (I) Plot density profiles demonstrating PSD-95 clustering of Kv1.3. (II) Plot density profiles demonstrating PSD-95 clustering of non-conducting Kv1.3 mutant, W386F Kv1.3. (III) Plot density profiles demonstrating Kv1.3 clustering in the presence of PSD-95 and IR kinase. (IV) Representative field of view of HEK293 cell morphology following co-transfection of Kv1.3 and PSD-95 cDNA. Red channel = αKv1.3. Green channel = αPSD-95. Merged image = yellow. Arrow = clustered channel signal; independent of cell morphology. Scale bar = 10 μm.

with species–specific antisera to determine the expression pattern and co-localization of all three proteins. Confocal imaging of sections showed that Kv1.3 and IR kinase co-localize in the soma of the MT cell layers, as well as synaptic processes within the glomerular layer and external plexiform layer (Fig. 9a and b). We used a transgenic line of mice created in the Sanes' laboratory designed for neural yellow fluorescent protein labeling of MT cell (Feng *et al.* 2000) to better determine if labeling of these proteins localized within MT cell dendrites and their projections. Using these reporter mice, we could visualize Kv1.3 and PSD-95 co-localization within MT cell axons in the granule cell layer, approximately

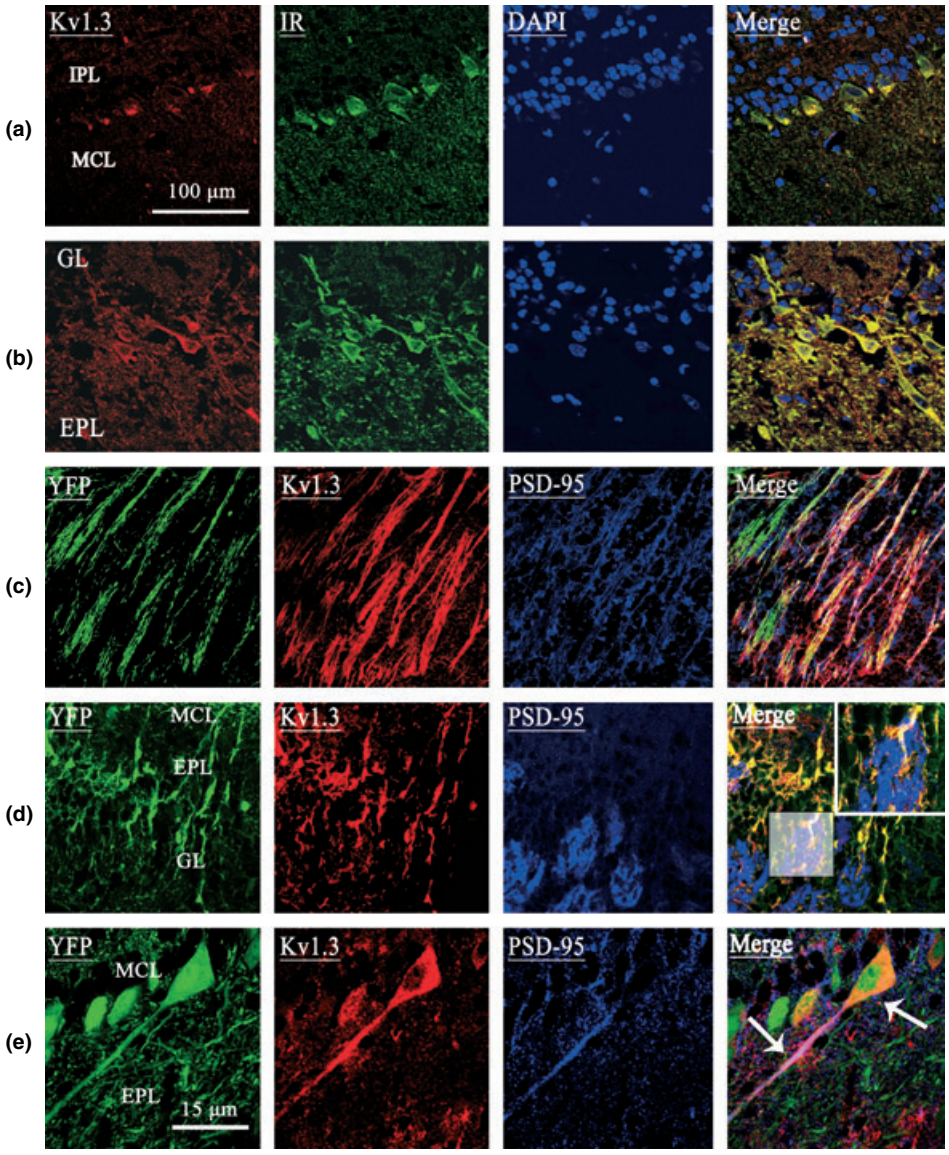

Fig. 9 Kv1.3 channel, post-synaptic density 95 (PSD-95) adaptor protein, and IR receptor tyrosine kinase co-localization across the neural lamina of the mouse olfactory bulb. (a–e) Confocal photomicrographs of the olfactory bulb, sectioned coronally, acquired from postnatal day 20 wildtype (a and b) or YFP-mitral cell labeled mice (c–e). Sections were labeled with primary antibodies for either Kv1.3, IR kinase, or PSD-95 and visualized with species–specific secondary antisera; protein labels are color-coded in conjunction with the observed reflected light following applied excitation spectra. Some sections were also stained with the nuclear marker DAPI. The final panel in each row represents the merged image of two to three channels (white). MCL, mitral cell layer; IPL, internal plexiform layer; EPL, external plexiform layer; GL, glomerular layer. Scale bar = 100 μm (a–d) or 15 μm (d inset and e).

800–1000 μm deep into the OB (Fig. 9c). Figure 9d demonstrates a region in which channel and adaptor protein were co-localized in the MT cell layers dendrites whereas the majority of PSD-95 label was isolated to the glomeruli, which did not overlap with that of Kv1.3 (box denotes region of higher magnification displayed in the inset). Finally, 100X magnification resolved subcellular distribution of PSD-95 and Kv1.3 in single MT cell, where somatic Kv1.3 expression did not overlap with PSD-95 but the two were strongly co-localized in a dendritic process (Fig. 9e). Kv1.3, IR kinase, and PSD-95 were also co-localized in the internal plexiform and granule cell layers but to a lesser extent (data not shown).

Discussion

The molecular interactions of PDZ domain-containing adaptor proteins with both ligand- and voltage-gated ion channels

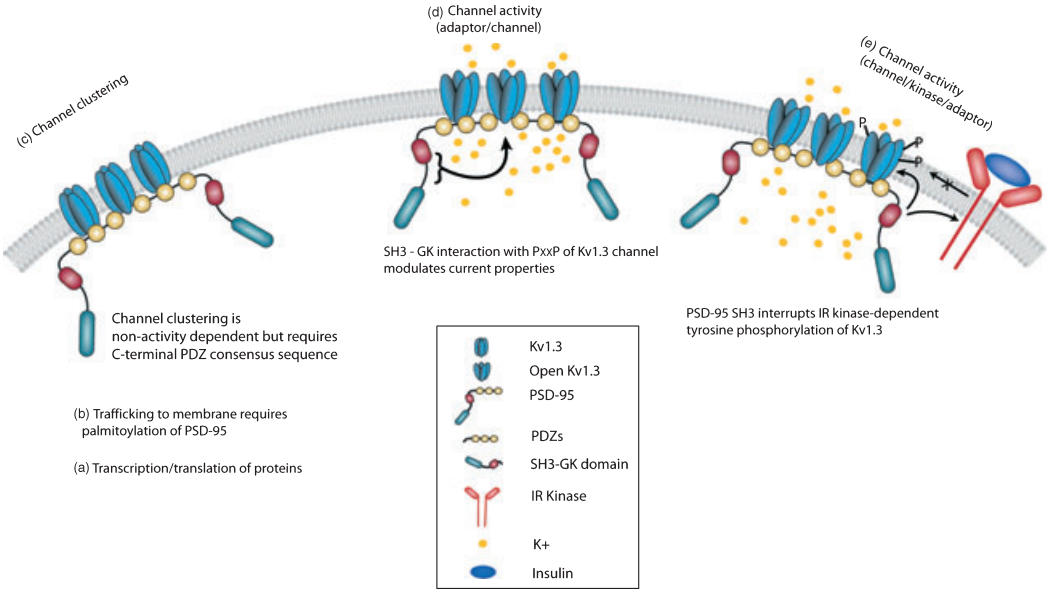

Fig. 10 Schematic of Kv1.3/post-synaptic density 95 (PSD-95) versus Kv1.3/IR kinase/PSD-95 interactions. (a) Proteins are transcribed and translated, followed by required (b) palmitoylation of PSD-95 for proper adaptor membrane trafficking. (c) PSD-95 clustering of Kv1.3 requires the channel C-terminal PDZ recognition motif, but does not depend upon channel activity. (d) Kv1.3 activity then permits the PSD-95 SH_3–GK domain modulation of channel current properties. (e) If IR kinase is present, the PSD-95 SH_3 domain has the capacity to disrupt IR kinase-dependent tyrosine phosphorylation and current suppression of Kv1.3. Cartoon representations as denoted in the box.

have been well characterized to organize signal transduction pathways in the cell via receptor/channel surface targeting, cytoskeletal anchoring, and clustering. There is a wealth of research that supports PSD-95 clustering of NMDA receptors and *Shaker* ion channels that incorporates mutagenesis and imaging approaches to delineate the precise interactive domains between the adaptor and receptor/channel. Much less is known, however, about the biophysical or functional correlates of the protein–protein interactions. Moreover, how the assembly of PSD-95 in a scaffolding complex affects modulation of ion channels is also poorly understood. Our study demonstrates that modulation of Kv1.3 by PSD-95 is not solely dependent upon prototypical interactions with the PDZ domains of PSD-95, but additionally the SH_3–GK domain can modulate current magnitude, inactivation kinetics, and cumulative inactivation (see Fig. 10). Modulation of the channel is not strictly coupled to PSD-95-induced channel clustering nor is it dependent upon a protein–protein interaction observed by co-immunoprecipitation. Secondly, we demonstrate that kinase-induced (IR) modulation of Kv1.3 current suppression is disrupted by PSD-95. IR kinase-induced channel suppression occurs in the absence of a direct Kv1.3/IR kinase protein–protein interaction (Fadool and Levitan 1998; Fadool *et al.* 2000), but can be disrupted when PSD-95 scaffolds with the Kv1.3 channel. The disruption of IR kinase-induced channel modulation is correlated to the formation a Kv1.3/IR kinase/PSD-95 complex that prevents Kv1.3 tyrosine phosphorylation. Deletion of the SH_3 domain restores insulin-stimulated tyrosine phosphorylation of the channel, IR kinase-induced channel suppression, and uncouples IR kinase clustering in the presence of Kv1.3/PSD-95. These data have important implications for insulin as an endocrine hormone with dual function to modulate electrical activity. We have shown that expression of IR kinase is activity dependent and can be suppressed with odor-sensory deprivation to the OB (Fadool *et al.* 2000). Data from our current study now suggest another tier of regulation, in that the presence of PSD-95 can block or reciprocally regulate insulin modulation of Kv1.3 that might be up-regulated with activity or metabolism.

Voltage-gated *Shaker* potassium channels have been shown to co-IP with PDZ-containing proteins in non-neuronal cells (T lymphocytes), heterologous expression systems, or via glutathione-S-transferase *in vitro* pull-down assays (Kim and Sheng 1996; Hanada *et al.* 1997; Cayabyab *et al.* 2000; Eldstrom *et al.* 2002). It was anticipated, therefore, that Kv1.3 in our hands, would co-IP with PSD-95 as transiently expressed in HEK293 cells. What was unexpected was that while the channel and adaptor formed a protein–protein interaction that presumably permitted clustering of Kv1.3, the functional modulation of current properties was not restricted to PSD-95 contact with the channel via its PDZ recognition motif nor was it coupled to the adaptor's ability to cluster the channel. Shin *et al.* (2000) report that disruption of the PSD-95 SH_3–GK intramolecular reaction impairs the ability of PSD-95 to cluster the Kv1.4 channel. Although we report that removal of the GK or the SH_3–GK domain of PSD-95 fails to disrupt any clustering of

Kv1.3, the intramolecular reaction of the SH_3 and GK domains may very well be needed to modulate Kv1.3 biophysics. The removal of the SH_3–GK domain of PSD-95 abolishes all modulatory activity that PSD-95 exerts on Kv1.3. Secondarily, while the SH_3–GK domain governs modulation of channel kinetics and current magnitude and not direct clustering between the adaptor and channel, clustering Kv1.3 may make the channels more easily accessible by adaptor proteins and tyrosine kinases, and thus may serve as an indirect form of neuromodulation in the OB.

While PSD-95 has been found to suppress internalization or surface targeting of two other *Shaker* family members (Kv1.4, Kv1.5), co-expression of PSD-95 had no functional effects on current or kinetic properties of these channels such as we observed for Kv1.3 (Jugloff *et al.* 2000; Eldstrom *et al.* 2002). Our discovered PSD-95 modulation of Kv1.3 may be linked to the strong use-dependent inactivation of this channel compared with other *Shaker* family members. Unlike Kv1.4 channels that underlie A-type, delayed-rectifier currents and which have rapid N-type inactivation properties, Kv1.3 has a slower C-type inactivation and a very slow exit rate from the inactivated state (Levy and Deutsch 1996). One would conjecture that the presumably large bulkhead created by PSD-95 binding onto the Kv1.3 channel, or potentially multimers of channel and adaptor complexing together, could conformationally disturb the channel over time to cause the observed decrease in τ_{inact}. The voltage paradigms described for Kv1.4 and Kv1.5 are calculated to have taken only 6 min and < 1 min, respectively, compared with our repetitive voltage stimulation over the course of 30 min. It is noteworthy that without repetitive stimulation (T_s = 45 s, 35x) PSD-95-induced Kv1.3 current suppression and decreased τ_{inact} kinetics was not observed. Repeated depolarizations of the Kv1.3-containing MT cells in the OB by activity-dependent odor stimulation of olfactory sensory neurons (OSNs) (sniffing), could lead to repeated opening and closing of the Kv1.3 channel. Behavioral tasks requiring continual use of the olfactory system (i.e. odor tracking or discrimination) could induce such a repetitive use of Kv1.3. In turn, subsequent current suppression by PSD-95 would be expected to induce an overall increase in membrane excitability.

Mechanistically, the modulation of Kv1.3 by PSD-95 might also be inherent to the structure of the C-terminus of most *Shaker* channels in combination with activity dependence. Magidovich *et al.* (2006) report that this portion of the K channel is intrinsically disordered and may operate by a 'fishing rod-like' mechanism. In this model, the constant movement of the C-terminal segment is proposed to increase the likelihood that the PDZ recognition motif will find and bind to a PDZ domain of PSD-95. Once the C-terminal segment of the channel has an effective collision with the PSD-95 PDZ domain and is complexed with the channel, the adaptor would presumably be in close molecular range to interact with the channel's proline rich motifs via the SH_3–GK domain. Our data do not distinguish if PSD-95/channel complex (co-immunoprecipitation) is promoted by opening and closing of the channel, but we do know that modulation is activity dependent. Interestingly, clustering of Kv1.3 by PSD-95, however, is not dependent upon ion conduction. Our HEK293 experiments show that after 30–36 h, Kv1.3 shows robust clustering and co-localization with PSD-95 in the HEK293 cell membrane as well as strong clustering of the non-conducting channel mutant, W386F Kv1.3. W386F Kv1.3 has been shown to have a gating current but does not conduct potassium (Perozo *et al.* 1993). Kv1.3 channel clustering is thus largely independent of activity while modulation of Kv1.3 biophysics by PSD-95 is not.

Our results demonstrate that PSD-95 blocks insulin-evoked Kv1.3 current suppression; an effect that is reversed upon deletion of the SH_3 domain of PSD-95. The IR kinase has several proline-rich sequences on the beta chain, making it an excellent candidate for interaction with the SH_3 domain of PSD-95. These proline-rich motifs are within the catalytic domain of IR kinase, which if bound by PSD-95 SH_3 domain, could be inhibited by steric interactions and thus unable to phosphorylate Kv1.3 and suppress channel current. Another possibility is that PSD-95 physically prevents IR kinase from interacting with Kv1.3 by holding IR kinase in position away from the channel, thus separating the two proteins. This could be achieved by PSD-95 SH_3 domain interactions with the proline-rich sequences on Kv1.3 that are in close adjacency to its determined insulin tyrosine phosphorylation sites in both the N- and C-termini (Fadool and Levitan 1998; Fadool *et al.* 2000).

In native OB, the channel and the adaptor protein form a protein–protein interaction that we found is robust enough to be immunoprecipitated. Although formation of a complex does not appear to be functionally necessary to induce modulation of channel biophysics, interaction implicates close proximity in the native state to permit the modulation. The fact that all three proteins show overlapping expression in the neural lamina of the OB also suggests modulation of excitability by shunting K-channel conductance in these neurons. Glomeruli are the initial site of synaptic contact in the OB and provide a topographical map of incoming odorant sensory information i.e. (Rubin and Katz 1999). They receive direct input from axons of the OSNs, which transmit the external sensory information (odorant binding) received and transduced by the OSN olfactory receptors to the MT cell dendrites. Mice with gene-targeted deletion of Kv1.3 show marked reduction in glomerular size (Fadool *et al.* 2004) and changes in synaptic connections that may attribute to their altered olfactory ability (KC Biju, unpublished data). Modulation of Kv1.3 by RTK or adaptor proteins in MT cell dendrites would likely affect the manner in which information arriving from OSN axons is received and propagated to MT cell bodies. We also report here that Kv1.3, IR kinase, and PSD-95 are heavily expressed and co-localized in the granule

cell layer, an area that is known to modulate MT cell activity as well. Granule cells are axonless interneurons that mediate lateral inhibition of MT cells via the formation of unique reciprocal dendrodendritic synapses (Strowbridge and Isaacson 1998). There are dense synaptic connections in the internal plexiform as well as the granule cell layer. The granule cells-MT synapses are suggested to be regions where synaptic plasticity and long-term potentiation occurs (Satou *et al.* 2005). PSD-95 is well known for its role in long-term potentiation (Miguad *et al.* 1998), and it is not surprising that there is heavy expression in regions of large numbers of synapses. PSD-95 mRNA is expressed in every layer of the OB at P1. By P14, there are large amounts of mRNA expression in virtually every cell type of the OB (Shu *et al.* 2001).

The subcellular distribution that we observed for IR kinase, Kv1.3, and PSD-95 might suggest a novel fine tuning or compartmentalization of neuromodulation for the MT cell neurons. Our previous recordings of native Kv1.3 current in MT cell neurons took advantage of an *in vitro* cell culture preparation that facilitated insulin application (Fadool and Levitan 1998; Fadool *et al.* 2000). The fact that we previously only observed changes in current magnitude and not alterations in inactivation kinetics is likely due to the fact that native synaptic connections were not maintained in the culture dish and thus we cannot be certain if PSD-95 was ever localized in close adjacency to the native Kv1.3 channel. Our current immunocytochemical data demonstrate that IR kinase and Kv1.3 were co-localized in the soma of these neurons whereas Kv1.3 and PSD-95 were co-localized in the MT cell axons. One could envision a subcellular compartmentalization of Kv1.3 biophysics, therefore, dependent upon whether the kinase or adaptor directs the modulation as driven by subcellular proximity. In the MT cell dendrites, all three were co-localized, suggesting a still different pattern of modulation where PSD-95 would be predicted to block insulin-induced Kv1.3 current suppression. In fact, PSD-95 has been similarly been reported as a negative regulator of Src kinase-induced NMDA receptor activity (Kalia *et al.* 2006). While our reported images captured both regions of strong co-localization and distinct regions of non-overlapping expression of channel/kinase/adaptor complexes, it is important to underscore that neither the expression of PSD-95 nor IR kinase signaling would be expected to remain static in the OB or any brain region. Metabolic state, meal frequency, and circadian cycles are all known to influence IR kinase signaling (i.e. Heptulla *et al.* 2001) whereas new synapse formation, behavioral training, developmental disorders/disease, and ischemia are a few of the many factors that influence PSD-95 expression (i.e. Skibinska *et al.* 2001; Mizui *et al.* 2005; Pollak *et al.*, 2005; Wang *et al.* 2005; Clinton *et al.* 2006; Gorczyca *et al.* 2007). The final firing frequency and shape of the resultant action potential would be expected to be a summation of propagated current to the axon hillock but finely tuned by contributions from the combined Kv1.3 conductance. This degree of subcellular regulation of channel modulation could vary with both brain region and level of PSD-95 expression. Kv1.3 in the hippocampus is predominantly expressed in dendrites and weakly localized to the soma or axons, where the channel is thought to direct its subcellular expression but can be modified by increased PSD-95 expression (Arnold and Clapham 1999). Moreover, PSD-95 has been reported to modulate ion-channel clustering extrasynaptically (Amadesi *et al.* 2006), further supporting the complexity of ion-channel functional scaffolds.

Acknowledgements

We would like to thank Drs David Fedida (University of British Columbia) and Jeffery Martins (University of Michigan) for presenting PSD-95 cDNA constructs used in our study. We would like to thank Ms Kimberly Riddle for her expert technical training in dual photon microscopy in the Florida State University (FSU) Core Imaging Facility of the Biological Science Department. We thank Dr Roni Dhanarajan for construction of the proline and PDZ recognition site mutations in Kv1.3 performed in the FSU Molecular Core Facility of the Biological Science Department. We would also like to thank Ms Danielle Walker and Mr Robert Daly for routine technical assistance and laboratory management. We would like to thank Drs James Michael Fadool and Biju KC for insightful discussions concerning neural imaging. This work was supported by NIH grants DC03387 and F31DC008045 from the NIDCD and a Neuroscience Fellowship Award from the Robinson Family & Tallahassee Memorial Hospital.

References

Abramoff M. D., Magelhaes P. J. and Ram S. J. (2004) Image processing with ImageJ. *Biophotonics Int.* **11**, 36–42.

Amadesi S., Cottrell G. S., Divino L. *et al.* (2006) Protease-activated receptor 2 sensitizes TRPV1 by protein kinase C (epsilon)- and A-dependent mechanisms in rats and mice. *J. Physiol.* **575**, 555–571.

Arnold D. B. and Clapham D. E. (1999) Molecular determinants for subcellular localization of PSD-95 with an interacting K^+ channel. *Neuron* **23**, 149–157.

Balu R., Larimer P. and Strowbridge B. W. (2004) Phasic stimuli evoke precisely timed spikes in intermittently discharging mitral cells. *J. Neurophysiol.* **92**, 743–753.

Banks W. A., Kastin A. J. and Pan W. (1999) Uptake and degradation of blood-borne insulin by the olfactory bulb. *Peptides* **20**, 373–378.

Baskin D. G., Porte D. Jr, Guest K. and Dorsa D. M. (1983) Regional concentrations of insulin in the rat brain. *Endocrinology* **112**, 898–903.

Bockmann J., Kreutz M. R., Gundelfinger E. D. and Bockers T. M. (2002) ProSAP/Shank postsynaptic density proteins interact with insulin receptor tyrosine kinase substrate IRSp53. *J. Neurochem.* **83**, 1013–1017.

Bowlby M. R., Fadool D. A., Holmes T. C. and Levitan I. B. (1997) Modulation of the Kv1.3 potassium channel by receptor tyrosine kinases. *J. Gen. Physiol.* **110**, 601–610.

Brann J. H., Dennis J. C., Morrison E. E. and Fadool D. A. (2002) Type-specific inositol 1,4,5-trisphosphate receptor localization in the vomeronasal organ and its interaction with a transient receptor potential channel, TRPC2. *J. Neurochem.* **83**, 1452–1460.

Bruning J. C., Gautam D., Burks D. J. *et al.* (2000) Role of brain insulin receptor in control of body weight and reproduction. *Science* **289**, 2122–2125.

Burke N. A., Takimoto K., Li D., Han W., Watkins S. C. and Levitan E. S. (1999) Distinct structural requirements for clustering and immobilization of K^+ channels by PSD-95. *J. Gen. Physiol.* **113**, 71–80.

Cayabyab F. S., Khanna R., Jones O. T. and Schlichter L. C. (2000) Suppression of the rat microglia Kv1.3 current by src-family tyrosine kinases and oxygen/glucose deprivation. *Eur. J. Neurosci.* **12**, 1949–1960.

Clinton S. M., Haroutunian V. and Meador-Woodruff J. H. (2006) Up-regulation of the NMDA receptor subunit and post-synaptic density protein expression in the thalamus of elderly patients with schizophrenia. *J. Neurochem.* **98**, 1114–1125.

Colley B. S., Biju K. C., Visegrady A., Campbell S. and Fadool D. A. (2007) TrkB increases Kv1.3 ion channel half-life and surface expression. *Neuroscience* **144**, 531–546.

Colley B., Tucker K. and Fadool D. A. (2004) Comparison of modulation of Kv1.3 channel by two receptor tyrosine kinases in olfactory bulb neurons of rodents. *Recept. Channels* **10**, 25–36.

Cook K. K. and Fadool D. A. (2002) Two adaptor proteins differentially modulate the phosphorylation and biophysics of Kv1.3 ion channel by SRC kinase. *J. Biol. Chem.* **277**, 13268–13280.

Das P., Parsons A. D., Scarborough J., Hoffman J., Wilson J., Thompson R. N., Overton J. M. and Fadool D. A. (2005) Electrophysiological and behavioral phenotype of insulin receptor defective mice. *Physiol. Behav.* **86**, 287–296.

Dickson B. J. (2003) Wiring the brain with insulin. *Science* **300**, 440–441.

Doyle D. A., Lee A., Lewis J., Kim E. and Sheng M. (1996) Crystal structures of a complexed and peptide-free membrane protein-binding domain: molecular basis of peptide recognition by PDZ. *Cell* **85**, 1067–1076.

Eldstrom J., Doerksen K. W., Steele D. F. and Fedida D. (2002) N-terminal PDZ-binding domain in Kv1 potassium channels. *FEBS Lett.* **531**, 529–537.

El-Husseini A. E.-D., Schnell E., Chetkovich D. M., Nicoll R. A. and Bredt D. S. (2000) PSD-95 involvement in maturation of excitatory synapses. *Science* **290**, 1364–1368.

Ellis L., Clauswer E., Morgan D. O., Edery M., Roth R. A. and Rutter W. J. (1986) Replacement of insulin receptor tyrosine residues 1162 and 1163 compromises insulin-stimulated kinase activity and uptake of 2-deoxyglucose. *Cell* **45**, 721–732.

Fadool D. A. and Levitan I. B. (1998) Modulation of olfactory bulb neuron potassium current by tyrosine phosphorylation. *J. Neurosci.* **18**, 6126–6137.

Fadool D. A., Holmes T. C., Berman K., Dagan D. and Levitan I. B. (1997) Multiple effects of tyrosine phosphorylation on a voltage-dependent potassium channel. *J. Neurophysiol.* **78**, 1563–1573.

Fadool D. A., Tucker K., Phillips J. J. and Simmen J. A. (2000) Brain insulin receptor causes activity-dependent current suppression in the olfactory bulb through multiple phosphorylation of Kv1.3. *J. Neurophysiol.* **83**, 2332–2348.

Fadool D. A., Tucker K., Perkins R., Fasciani G., Thompson R. N., Parsons A. D., Overton J. M., Koni P. A., Flavell R. A. and Kaczmarek L. K. (2004) Kv1.3 channel gene-targeted deletion produces "Super-Smeller Mice" with altered glomeruli, interacting scaffolding proteins, and biophysics. *Neuron* **41**, 389–404.

Feng G., Mellor R. H., Bernstein M., Keller-peck C., Nguyen Q. T., Lichtman J. W. and Sanes J. R. (2000) Imaging neuronal subsets in transgenic mice expressing multiple spectral variants of GFP. *Neuron* **28**, 41–51.

Folli F., Bonfanti L., Renard E., Kahn C. R. and Merighi A. (1994) Insulin receptor substrate-1 (IRS-1) distribution in the rat central nervous system. *J. Neurosci.* **14**, 6412–6422.

Gerozissis K. (2003) Brain insulin: regulation, mechanisms of action and functions. *Cell. Mol. Neurobiol.* **23**, 1–25.

Gorczyca D., Ashley J., Speese S., Gherbesi N., Thomas U., Gundelfinger E., Gramates L. S. and Gudnik V. (2007) Postsynaptic membrane addition depends on the Discs-Large-interacting t-SNARE G-taxin. *J. Neurosci.* **27**, 1033–1044.

Graziadei P. P. C. and Monti-Graziadei G. A. (1978) Development of Sensory Systems, in *Handbook of Sensory Physiology* (Jacobson M., ed.), pp. 55. Springer, Berlin.

Gupta G., Azam M. and Baquer N. Z. (1992) Modulation of rat brain insulin receptor kinase activity in diabetes. *Neurochem. Int.* **20**, 487–492.

Hanada T., Lin L., Chandy K. G., Oh S. S. and Chishti A. H. (1997) Human homologue of the Drosophila discs large tumor suppressor binds to p56lck tyrosine kinase and Shaker type Kv1.3 potassium channel in T lymphocytes. *J. Biol. Chem.* **272**, 26899–26904.

Henke G., Maier G., Wallisch S., Boehmer C. and Lang F. (2004) Regulation of the voltage gated K^+ channel Kv1.3 by the ubiquitin ligase Nedd4-2 and the serum and glucocorticoid inducible kinase SGK1. *J. Cell. Physiol.* **199**, 194–199.

Heptulla R., Smitten A., Teague B., Tamborlane W. V., Ma Y.-Z. and Caprio S. (2001) Temporal patterns of circulating leptin levels in lean and obese adolescents: relationships to insulin, growth hormone, and free fatty acids rhythmicity. *J. Clin. Endo. Met.* **86**, 90–96.

Hill J. M., Lesniak M. A., Pert C. B. and Roth J. (1986) Autoradiographic localization of insulin receptors in rat brain: prominence in olfactory and limbic areas. *Neuroscience* **17**, 1127–1136.

Holmes T. C., Fadool D. A. and Levitan I. B. (1996a) Tyrosine phosphorylation of the Kv1.3 potassium channel. *J. Neurosci.* **16**, 1581–1590.

Holmes T. C., Fadool D. A., Ren R. and Levitan I. B. (1996b) Association of src tyrosine kinase with a human potassium channel mediated by SH3 domain. *Science* **274**, 2089–2091.

Holmes T. C., Berman K., Swartz J. E., Dagan D. and Levitan I. B. (1997) Expression of voltage-gated potassium channels decreases cellular protein tyrosine phosphorylation. *J. Neurosci.* **17**, 8964–8974.

Imamura F., Maeda S., Doi T. and Fujiyoshi Y. (2002) Ligand binding of the second PDZ domain regulates clustering of PSD-95 with the Kv1.4 potassium channel. *J. Biol. Chem.* **277**, 3640–3646.

Iwamoto T., Yamada Y., Hori K., Watanabe Y., Sobue K. and Inui M. (2004) Differential modulation of NR1-NR2A and NR1-NR2 subtypes of NMDA receptor by PDZ domain-containing proteins. *J. Neurochem.* **89**, 100–108.

Jugloff D. G. M., Khanna R., Schlichter L. C. and Jones O. T. (2000) Internalization of the Kv1.4 potassium channel is suppressed by clustering interactions with PSD-95. *J. Biol. Chem.* **275**, 1357–1364.

Kahn C. R. (1996) Insulin action, diabetogenes, and the cause of type II diabetes. *Diabetes* **443**, 1084.

Kalia L. V. and Salter M. W. (2003) Interactions between Src family protein tyrosine kinase and PSD-95. *Neuropharmacology* **45**, 720–728.

Kalia L. V., Pitcher G. M., Pelkey K. A. and Salter M. W. (2006) PSD-95 is a negative regulator of the tyrosine kinase Src in the NMDA receptor complex. *EMBO J.* **25**, 4971–4982.

Kennedy M. B. (2000) Signal-processing machines at the postsynaptic density. *Science* **290**, 750–754.

Kim E. and Sheng M. (1996) Differential K^+ channel clustering activity of PSD-95 and SAP97, two related membrane-associated putative guanylate kinases. *Neuropharmacology* **35**, 993–1000.

Kim E., Niethammer M., Rothchild A., Yan Y. N. and Sheng M. (1995) Clustering of Shaker-type K^+ channels by interaction with a family of membrane-associated guanylate kinases. *Nature (London)* **378**, 85–88.

Kornau H.-C., Schenker L. T., Kennedy M. B. and Seeburg P. H. (1995) Domain interaction between NMDA receptor subunits and the postsynaptic density protein PSD-95. *Science* **269**, 1737–1740.

Kupper J., Bowlby M. R., Marom S. and Levitan I. B. (1995) Intracellular and extracellular amino acids that influence C-type inactivation and its modulation in a voltage-dependent potassium channel. *Pflugers Arch.* **430**, 1–11.

Lee Y. H. and White M. F. (2004) Insulin receptor substrate proteins and diabetes. *Arch. Pharm. Res.* **27**, 361–370.

Levy D. I. and Deutsch C. (1996) A voltage-dependent role for K^+ in recovery from C-type inactivation. *Biophys. J.* **71**, 3157–3166.

Magidovich E., Fleishman S. J. and Yifrach O. (2006) Intrinsically disordered C-terminal segments of voltage-activated potassium channels: a possible fishing rod-like mechanism for channel binding to scaffold proteins. *Bioinformatics* **22**, 1546–1550.

Marom S. and Levitan I. B. (1994) State-dependent inactivation of the Kv3 potassium channel. *Biophys. J.* **67**, 579–589.

Matsumoto H. and Rhoads D. E. (1990) Specific binding of insulin to membranes from dendrodendritic synaptosomes of rat olfactory bulb. *J. Neurochem.* **54**, 347–350.

McGee A. W., Dakoji S. R., Olsen O., Bredt D. S., Lim W. A. and Prehoda K. E. (2001) Structure of the SH3-guanylate kinase module from PSD-95 suggests a mechanism for regulated assembly of MAGUK scaffolding proteins. *Mol. Cell* **8**, 1291–1301.

Miguad M., Charlesworth P., Dempster M. *et al.* (1998) Enhanced long-term potentiation and impaired learning in mice with mutant postsynaptic density-95 protein. *Nature (London)* **396**, 433–439.

Mittman S. C., Flaming D. G., Copenhagen D. R. and Belgum J. H. (1987) Bubble pressure measurement of micropipet tip outer diameter. *J. Neurosci. Methods* **22**, 161–166.

Mizui T., Takahashi H., Sekino Y. and Shirao T. (2005) Overexpression of drebrin A in immature neurons induces the accumulation of F-actin and PSD-95 into dendritic filopodia, and the formation of large abnormal protrusions. *Mol. Cell Neurosci.* **30**, 630–638.

Myers M. G. Jr and White M. F. (1993) The new elements of insulin signaling: insulin receptor substrate-1 and proteins with SH2 domains. *Diabetes* **42**, 643–650.

Neubauer N. and Kulkarni R. N. (2006) Molecular approaches to study control of glucose homeostasis. *ILAR J.* **47**, 199–211.

Nitabach M. N., Llamas D. A., Thompson I. J., Collins K. A. and Holmes T. C. (2002) Phosphorylation-dependent and phosphorylation-independent modes of modulation of shaker family voltage-gated potassium channels by SRC family protein tyrosine kinases. *J. Neurosci.* **22**, 7913–7922.

Panyi G., Sheng Z. and Deutsch C. (1995) C-type inactivation of a voltage-gated K^+ channel occurs by a cooperative mechanism. *Biophys. J.* **69**, 896–903.

Perozo E., MacKinnon R., Benzanilla F. and Stephani E. (1993) Gating currents from a non-conducting mutant reveal open-closed conformations in Shaker channels. *Neuron* **11**, 353–358.

Pollak D. D., Herkner K., Hoeger H. and Lubec G. (2005) Behavioral testing upregulates PCaMKII, BDNF, PSD-95 and egr-1 in hippocampus of FVBIN mice. *Behav. Brain Res.* **163**, 128–135.

Ponting C. P., Phillips C., Davies K. E. and Blake D. J. (1997) PDZ domains: targeting signaling molecules to sub-membranous sites. *Bioessays* **19**, 469–479.

Rasband W. S. (2005) *ImageJ*. U.S. National Institutes of Health, Bethesda, MD, USA. Internet Communication, http://rsb.info.nih.gov/ij/

Reese M. L., Dakoju S., Bredt D. S. and Dötsch V. (2007) The guanylate kinase domain of MAGUK PSD-05 binds dynamically to a conserved motif in MAP1a. *Nat. Struct. Mol. Biol.* **14**, 155–163.

Rubin B. D. and Katz L. C. (1999) Optical imaging of odorant representations in the mammalian olfactory bulb. *Neuron* **23**, 499–511.

Satou M., Anzai S. and Huruno M. (2005) Long-term potentiation and olfactory memory formation in the carp (*Cyprinus carpio L.*) olfactory bulb. *J. Comp. Physiol. A Neuroethol. Sens. Neural Behav. Physiol.* **191**, 421–434.

Sheng M. (1997) Glutamate receptors put in their place. *Nature (London)* **386**, 221–222.

Sheng M. and Pak D. T. (2000) Ligand-gated ion channel interactions with cytoskeletal and signaling proteins. *Annu. Rev. Physiol.* **62**, 755–778.

Sheng M. and Wyszynski M. (1997) Ion channel targeting in neurons. *Bioessays* **19**, 847–853.

Shin H., Hsueh Y.-P., Yang F.-C., Kim E. and Sheng M. (2000) An intramolecular interaction between Src homology 3 domain and guanylate kinase-like domain required for channel clustering by postsynaptic density-95/SAP90. *J. Neurosci.* **20**, 3580–3587.

Shu F., Ohno K., Wang T., Kuriyama K., Ueki T., Kanayama N. and Sato K. (2001) Developmental changes in PSD-95 and Narp mRNAs in the rat olfactory bulb. *Brain Res. Dev. Brain Res.* **132**, 91–95.

Skibinska A., Lech M. and Kossut M. (2001) PSD-95 protein level rises in murine somatosensory cortex after sensory training. *Neuroreport* **12**, 2907–2910.

Songyang Z., Fanning A. S., Fu C., Xu J., Marfatia S. M., Chishti A. H., Crompton A., Chan A. C., Anderson J. M. and Cantley L. C. (1997) Recognition of unique carboxyl-terminal motifs by distinct PDZ domains. *Science* **275**, 73–77.

Strowbridge B. W. and Isaacson J. S. (1998) Olfactory reciprocal synapses: dendritic signaling in the CNS. *Neuron* **20**, 749–761.

Sun X. J., Rothenberg P., Kahn C. R., Backer J. M., Araki E., Wilden P. A., Cahill D. A., Goldstein B. J. and White M. F. (1991) Structure of the insulin receptor substrate IRS-1 defines a unique signal transduction protein. *Nature (London)* **352**, 73–77.

Takahashi S. X., Miriyala J., Tay L. H., Yue D. T. and Colecraft H. M. (2005) A CaVBeta SH3/guanylate kinase domain interaction regulates multiple properties of voltage-gated Ca2+channels. *J. Gen. Physiol.* **126**, 365–377.

Tavares G. A., Panepucci E. H. and Brunger A. T. (2001) Structural characterization of the intramolecular interaction between the SH3 and guanylate kinase domains of PSD-95. *Mol. Cell* **8**, 1313–1325.

Tiffany A. M., Manganas L. N., Kim E., Hsueh Y.-P., Sheng M. and Trimmer J. S. (2000) PSD-95 and SAP97 exhibit distinct mechanisms for regulating K^+ channel surface expression and clustering. *J. Cell Biol.* **148**, 147–157.

Tucker K. and Fadool D. A. (2002) Neurotrophin modulation of voltage-gated potassium channels in rat through TrkB receptors is time and sensory experience dependent. *J. Physiol.* **542**, 413–429.

Wang Q., Chen S. Y., Xiong L. Z., Jin W. L. and Yang J. (2005) Neuroprotective effect of sodium ferulate on transient focal cerebral ischemia by weakening activation of postsynaptic density-95 in rats. *J. Traumatol.* **8**, 297–302.

White M. F. (1997) The insulin signalling system and the IRS proteins. *Diabetalogia* **40**, S2–S17.

White M. F. (2003) Insulin signaling in health and disease. *Science* **302**, 1710–1711.

Wickelgren I. (1998) Tracking insulin to the mind. *Science* **280**, 517–519.

Yaffe M. B. (2002) MAGUK SH3 domains – swapped and stranded by their kinases? *Structure* **10**, 3–9.

Yellen G. (2002) The voltage-gated potassium channels and their relatives. *Nature (London)* **419**, 35–42.

Young W. S., Kuhar M. J., Roth J. and Brownstein M. J. (1980) Radiohistochemical localization of insulin receptors in The adult and developing brain. *Neuropeptides* **1**, 15–22.

